Design and Analysis of a Solar Assisted Absorption Cooling System Integrated with Latent Heat Storage

Name : Laleh Hosseini

Student Number: 4056345

Report Number: P&E - 2465

Master : Sustainable Process and Energy Technology

Delft University of Technology

August 2011

Author

Name Laleh Hosseini

Master Sustainable Process and Energy Technology

Student Number 4056345

E-mail L.hosseini@student.tudelft.nl

Company

Deerns consulting engineers

Fleminglaan 10

2289 CP Rijswijk

Supervisors

Dr.ir. C.A. Infante Ferreira

Dr.ir. P.J.W. van den Engel

Graduation committee

Prof.dr.ir. T.J.H. Vlugt (Chairman)

Dr.ir. C.A. Infante Ferreira

Dr. L.C.M. Itard

Dr.ir. P.J.W. van den Engel

Ir. J. van Dorp

Abstract

Air conditioning is one of the major consumers of electrical energy in many parts of the world. The demand can be expected to increase because of the changing working times, increased comfort expectations and global warming. With more air conditioning units, the electricity demand has been rising thereby increasing the use of fossil fuels and nuclear energy. A drastic change, therefore, should be implemented in the energy structure of the developed countries. Environmentally friendly and energy efficient technologies should be introduced in which the environmental impact of the conventional air conditioning system is minimized.

Solar radiation as a sustainable energy resource is one of the most available forms of energy on the earth surface which could reduce the fossil fuel consumption and CO_2 emission to the atmosphere. Solar cooling is a possible technological alternative to conventional air conditioning systems that has recently attracted a growing interest. A solar assisted absorption cooling system as a sustainable solution for cooling systems could provide both heating and cooling of a building. Since the solar energy is available for only a fraction of the day and its availability depends on several factors such as latitude and sky clearness, the storage of it is an important concern. Thermal energy storage is a practical way in conserving the solar energy as it can reduce the discrepancy between the energy supply and demand. Latent heat storage units (LHSU) using Phase Change Materials (PCMs) are promising candidates as heat storage media.

In this thesis, the behavior of a solar assisted single effect absorption system integrated with LHSU was investigated. The mathematical model for the single effect absorption system and the LHSU based on the mass and energy balances and heat transfer equations were developed. The models were implemented in MATLAB and the numerical results were validated with the experimental results from the literature. Based on the cooling demand of a specific building (waiting room in Schiphol airport) the absorption system and the LHSU were designed and the behavior of each system for different control parameters is investigated. For the designed single effect absorption system, variation of the COP and the evaporator heat transfer rate at the different flow rates and temperatures of the external cool water, hot water and the chilled water were studied. The results show that the chilled, hot and cooled water temperatures have significant effect on the performance of the absorption system. For the designed latent heat storage, several numerical investigations were conducted. The impact of the key parameters e.g. the mass of PCM, the number of tubes inside the PCM container and the radius of the tubes, on the thermal performances of the latent heat storage and the melting time duration were studied.

The behavior of the designed latent heat storage unit in charging process with varying solar collector field area was studied subsequently. The discharging process of LHSU for the maximum cooling demand of the building was investigated. It was observed that the designed LHSU could provide the requested hot water temperature for more than 10 hours which is sufficient for driving the air conditioning system.

Acknowledgments

In the first place, I would like to thank my supervisor at TU Delft, Dr. C.A. Infante Ferreira for his supervision, valuable technical advice and guidance from the early stage of the project.
I would like to acknowledge Deerns for the financial support of this project. Also my appreciation to my supervisors at Deerns, Dr. P.J.W. van den Engel and Mr. J. van Dorp for their advice and support during my research program. I wish to thank all my colleagues at the Deerns, building physics department, for making a friendly atmosphere.
I would like to thank my friends Pejman, Santosh and Sinyun for being such nice friends during the two years of my master program.
I am grateful for Dr. L. C.M. Itard for her Indoor Climate Control lecture which interested me in doing research in air conditioning systems.
My parents deserve special mention for their inseparable support and prayers. Words fail me to express my feeling and appreciation to them. Without their support and help I would not be in this position.
Finally, I owe special gratitude to my husband, Pooria, for continues, unconditional support and motivation he gave me during my studies.

Table of Contents

List of Figures

List of Tables

List of Symbols, Abbreviations and Nomenclature

Nomenclature

$\dot{m}_f$	Mass flow rate of the HTF, kg/s
A	Area, m^2
a_1	Loss conversion, $kW.m^{-2}.K$
a_2	Loss conversion, $kW.m^{-2}.K^2$
COP	Coefficient Of Performance
C_P	Specific heat capacity at constant pressure ,kJ/kg. K
D	Diameter
f	Mass flow rate, kg/s
G	Solar radiation, kW/m^2
h	Enthalpy, kJ/kg
HTF	Heat Transfer Fluid
k	Thermal conductivity , kW/m. k
L	Length, m
LHSU	Latent Heat Storage Unit
n	Time level
N_p	Number of pipes
Nu	Nusselt Number
P	Pressure (K.pa)
PCM	Phase Change Material
Pr	Prantel Number
Q	Heat transfer rate, kW
q	Vapor quality
R	Radial coordinate
R	Outside radius, m
r_0	Inside radius, m
Re	Reynolds Number
T	Temperature, ^oC
t	Time, s
T_{m1}	Lower melting temperature of PCM, ^oC
T_{m2}	Higher melting temperature of PCM, ^oC
U	Overall heat transfer coefficient, $kW/m^2.K$
V	Volume, m^3
$V_{j,k}$	Control element volume, m^3
W	Power, kW
X	LiBr concentration, percent by weight in solution %
Z	Axial coordinate
λ	Convective heat transfer coefficient, kW/m^2 k

Super- and subscripts

1, 2 …	State points
a	Absorber
amb	Ambient
c	Condenser
comp	Compressor
cool	Cooling
e	Evaporator
f	Heat transfer fluid
g	Generator
heat	Heating
in	Inlet
l	Liquid
m	Medium, Melting
out	Outlet
p	Pump
P	Phase change material
s	solid
v	Vapor

Greek symbols

ΔH	Latent heat, kJ/kg
ΔR	Radial space step, m
Δt	Time step, s
ΔT_{lm}	Logarithmic mean temperature difference, K
Δz	Axial space step, m
μ	Dynamic viscosity, kg/m s
ε	Heat exchanger effectiveness
η	Efficiency
η_0	Conversion factor
ρ	Density, kg/m^3

Chapter 1

Introduction

1.1 Introduction

The request for new technologies due to the environmental problems, the energy shortage and the high cost of energy have been a scientific concern over the last three decades. In recent years, the use of renewable energy such as solar, wind, geothermal and biomass energy has received considerable attention for domestic and industrial applications. Using solar energy systems is a promising mean of reducing the fossil fuel consumption and reducing the CO_2 emission into the atmosphere. Solar energy has two shortcomings: intermittence and dispersion. So, efficient and economical heat storage is a most important factor in the utilization of solar energy. Phase Change energy storage Materials (PCM) have proved to have a great potential in solar energy applications. Unlike sensible storage materials, such as water, masonry or rocks, PCM stores much more heat per unit volume and another key advantage with the use of a PCM is that heat storage and its recovery occurs isothermally, which makes them ideal for space heating/ cooling applications (Tyagi and Buddhi, 2007).

Air conditioning is one of the major consumers of electricity which increases the use of fossil fuels and CO_2 emissions. So far, a respectful number of investigations have been done on solar assisted heat pump systems with thermal storage. Kaygusuz developed an experimental model to determine the dynamics of a solar assisted heat pump, collectors, dryer, and energy storage tank used for drying grains. He also investigated the performance of a dual- source heat pump system for residential heating (Kaygusuz, 1995b). Kaygusuz conducted an experimental and theoretical study to determine the performance of phase- change energy storage materials, and the variation of the outlet fluid temperature with different values of NTU (number of transfer units for storage unit) for a solar water heating system (Kaygusuz, 1995a). Esen investigated the cylindrical phase change storage tank linked to a solar powered heat pump system both experimentally and theoretically (Esen, 2000). Qi et al. (2008) investigated the operational performances of a solar heat pump heating system with seasonal latent heat thermal storage.

The cooling potential of a mechanical ventilation system can be improved by the integration of short term latent heat thermal energy storage systems. Free cooling is the method of storing outdoors coldness during the night and supply to indoor air during the day. The main advantages of free cooling are cooling with reduction of the emission of greenhouse gases and excellent indoor air quality maintenance inside the building.

Raj and Velraj presented a detailed review on free cooling and the major challenges and facts posed in the use of PCM for system design such as thermal resistance of air and PCM and geometry of encapsulation (Raj and Velraj, 2010).

Stritih and Butala conducted an experimental analysis of cooling buildings by using night-time cold accumulation in a phase change material (PCM) (Stritih and Butala, 2007).

Zhang and Niu conducted an experimental study of microencapsulated paraffin slurry as cooling storage medium for building cooling applications (Zhang and Niu, 2010).

One of the methods for cooling buildings with solar energy is by use of an absorption refrigeration unit. Fong et al. did a comparative study of different solar cooling systems for buildings in a subtropical city. Through their study it is found that solar electric compression refrigeration and solar absorption refrigeration had the highest energy saving potential in subtropical Hong Kong (Fong *et al.*, 2010).

In order that solar air conditioning system can be available at lowest cost, it is essential that the system can be used both for cooling in summer and for heating in winter. There is not that much investigation done on combined solar cooling and heating systems (Löf and Tybout, 1974; Helm *et al.*, 2009).

In this chapter the phase change materials will be introduced and the selection of the solar assisted air conditioning system integrated with latent heat storage will be motivated.

1.2 Phase Change Material

PCMs are “latent” heat storage materials. They use chemical bonds to store and release the heat. The thermal energy transfer occurs when a material changes from solid to liquid, or liquid to solid. This is called a change in state or phase.

So far, a respectful number of investigations have been done on PCM. The properties of PCM to be used for latent heat storage were highlighted by (Schröder and Gawron, 1981) as follows:

- High value of the heat of fusion and specific heat per unit volume and weight,
- Melting point which matches the application,
- Low vapor pressure at the operational temperature,
- Chemical stability and non-corrosiveness,
- Should not be hazardous, highly inflammable or poisonous,
- Have a reproducible crystallization without degradation,
- Have a small supercooling degree and high rate of crystal growth,
- Have a small volume variation during solidification,
- A high thermal conductivity,
- A PCM should be of abundant supply and at a low cost.

Zalba et al. (2003) reviewed the 237 sources in the area of thermal energy storage using PCM's. One of the conclusions of this paper is that the thermo- physical properties have not been studied sufficiently in order that clear recommendation could be made for a design process of commercial heat storage units.
Kenisarin and Mahkamov analyzed the publications over the last 15 years on properties and application of PCMs and methods of enhancing heat and mass transfer in storage devices (Kenisarin and Mahkamov, 2007). Also Sharma et al. summarize the investigation and analysis of the available thermal energy storage systems incorporating PCMs for use in different applications (Sharma *et al.*, 2009).

1.3 Classifications of PCM

Complete reviews of the types of material which have been used, their classifications, advantages and disadvantages and the various experimental techniques which were used to determine the behavior of PCM in melting and solidification have been presented by Abhat (1983) and Lane (1983).

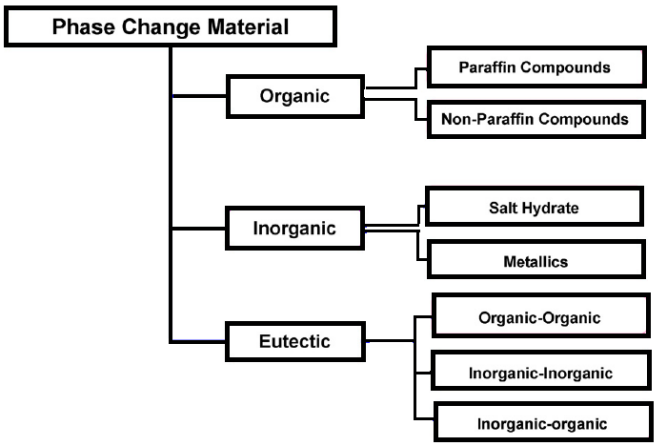

Figure 1.1 Classification of PCMs (Sharma et al., 2009)

Generally PCMs can be divided to three main types: Organic, Inorganic and Eutectic as it is shown in Figure 1.1. Among organic materials fatty acids which are in the non- paraffin group are the most attractive materials for PCM since they are relatively cheap and widely used in different areas. In solar heating systems the commercial paraffin and paraffin waxes are more attractive since these materials are produced in large quantities and widely used. They undergo negligible subcooling and are chemically inert and stable with no phase segregation.
Hydrated salts are the most attractive material among inorganic material and they have multiple applications in the field of solar energy storage (Lane, 1983; Dinçer and Rosen, 2011). Hydrated salts have high volumetric storage density (350 MJ/m^3), relatively high thermal conductivity (0.5 W/m K) and moderate costs compared to paraffin waxes, with few exceptions (Farid *et al.*, 2004). The problem with hydrated salts is their supercooling.
The chemical compounds and eutectic compositions are less attractive from the application point of view than the mixtures of commercially manufactured fatty acid products.

Zalba et al. (2003) compared the advantages and disadvantages of organic and inorganic materials which are shown in Table 1.1.

Table 1.1 Advantages and disadvantages of organic and inorganic PCMs

Organics	Inorganics
Advantages	**Advantages**
Not corrosives	Greater phase change enthalpy
Low or none undercooling	
Chemical and thermal stability	
Disadvantages	**Disadvantages**
Lower phase change enthalpy	Undercooling
Low thermal conductivity	Corrosion
inflammability	Phase separation
	Phase segregation, lack of thermal stability

Because phase change materials use 'phase change' to store energy, they can only be used in a limited temperature range. These temperature ranges can differ per each different kind of PCM, and within every type. The main selection criterion to decide on a specific PCM for storage medium is the phase change temperature. If this is not correctly chosen, the material cannot work properly. So as a first step the system configuration should be defined to select the PCM.

1.4 Description of the Building

The building is situated in the Amsterdam airport Schiphol in the Netherlands. It is a waiting room in terminal G of Schiphol airport with 400 m^2 which is in operation only 8 hours a day from 4 a.m. to 12 p.m. The maximum heating load and cooling load of the building are 33 kW and 72 kW, respectively, which are 82.5W/m^2 and 180 W/m^2. The energy load variation of the building is shown in Figure 1.2.

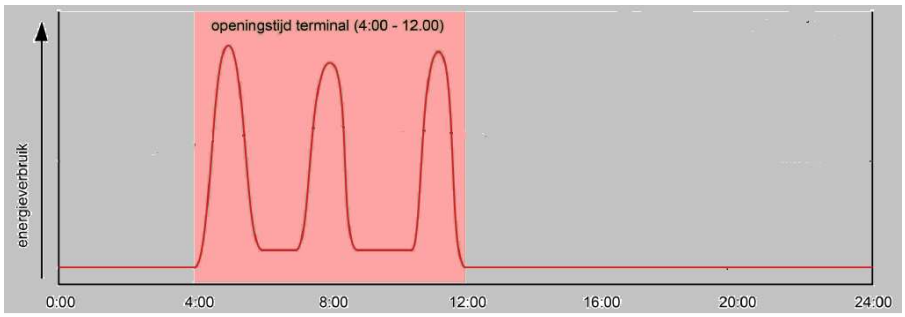

Figure 1.2 Energy load of the building in 24 hr

1.5 System Configurations

Different configurations were considered for cooling and heating the building. Four solutions are presented which are based on using solar thermal collectors and a PCM storage for storing the solar energy. In Figure 1.3 the different cases are shown and in the following sections each case will be explained in detail.

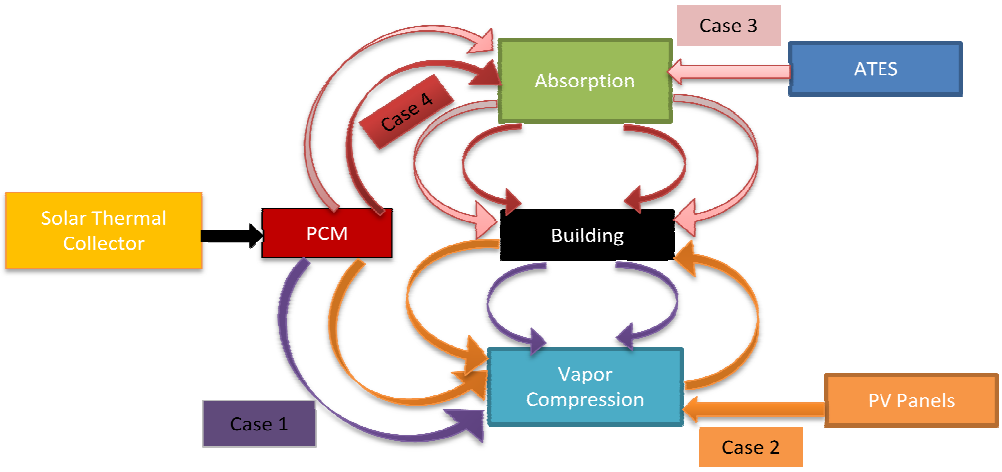

Figure 1.3 Different configurations for heating and cooling the system
ATES: Aquifer Thermal Energy Storage, PV panels: Photo Voltaic panels

1.5.1 Vapour compression system

Vapor compression (VC) air conditioners are composed of four basic components: evaporator, compressor, condenser and expansion valve, as shown in Figure 1.4.

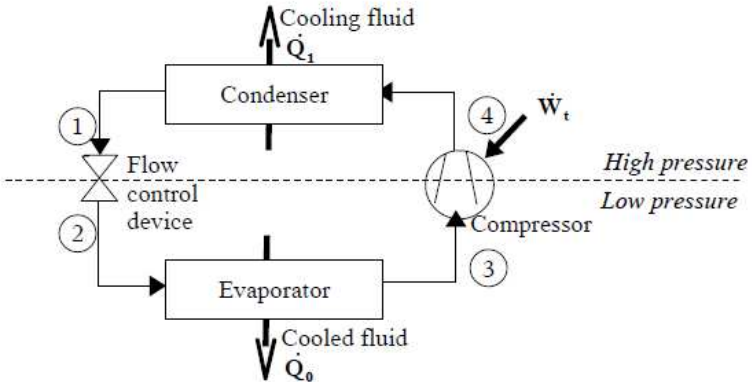

Figure 1.4 Vapor compression system

At point (1) the refrigerant in the liquid state at a relatively high pressure and high temperature flows to an expansion device. Exiting the expansion valve, the refrigerant pressure decreases that a small portion of the refrigerant vaporizes into a gas.
The refrigerant flows through an evaporator. The refrigerant absorbs heat from circulating fluid and vaporizes in to low pressure.

Leaving the evaporator the refrigerant is a gas at a low temperature and low pressure. In order to be able to use it again to achieve refrigerating effect continuously, it must be brought back to the conditions at (1).

The first step in this process is to increase the pressure of the refrigerant gas by the compressor. Compressing the gas also results in increasing its temperature. The refrigerant leaves the compressor as a gas at high temperature and pressure. In order to change it to a liquid, heat must be removed from it. This is accomplished in the condenser. Heat transfers from the refrigerant to the cooling fluid and, as a result, the refrigerant condenses to a liquid.

The Coefficient Of Performance (COP) of a vapor compression system is indicated as

$$COP_{cool} = \frac{Q_e}{W_{comp}} \quad \textbf{(1.1)}$$

$$COP_{heat} = \frac{Q_c}{W_{comp}} \quad \textbf{(1.2)}$$

The COP value of vapor compression systems for cooling seems to be from around 3 for smaller to medium size units and up to 4-5 for larger systems (Gordon and Choon Ng, 2000). The COP of the heat pump increases as the temperature difference between the heat source and application decreases. Figure 1.5 shows the COP of an ideal heat pump as a function of temperature lifts, where the temperature of heat source is 0^{o}C. Also shown is the range of actual COPs for various types and sizes of real heat pumps at different temperature lifts. The ratio of actual heat pump and ideal one is defined as Carnot Efficiency. The Carnot Efficiency varies from 0.3 to 0.5 for small electric heat pumps and 0.5 to 0.7 for large, high efficiency electrical heat pumps (Zogou and Stamatelos, 1998).

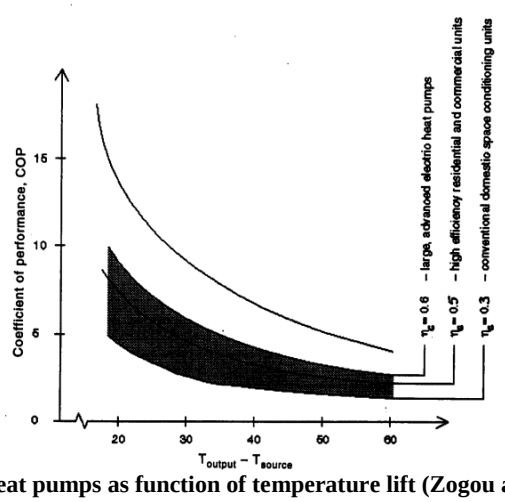

Figure 1.5 COP for heat pumps as function of temperature lift (Zogou and Stamatelos, 1998)

Two configurations could be considered for VC air conditioning systems with Latent Heat Storage (LHS). The configurations are explained in detail as follows.

Case1: Integrated VC system with solar thermal collector and LHS

In this system as it is shown in Figure 1.6, the solar thermal collector is integrated with a LHS and a VC system. In the cold season when it is needed to heat up the building, during the day the hot water flows through the storage and exchanges heat with PCM inside the LHS. The PCM absorbs the solar energy and melts. The hot fluid from the latent heat storage flows through the evaporator and evaporates the refrigerant. The refrigerant inside the evaporator coils vaporizes and flows through the compressor, and then the heating water flow through the condenser exchanges heat with the refrigerant and, with higher temperature, flows through the building.

During the night the PCM exchanges heat with the cold water from the evaporator and solidifies.

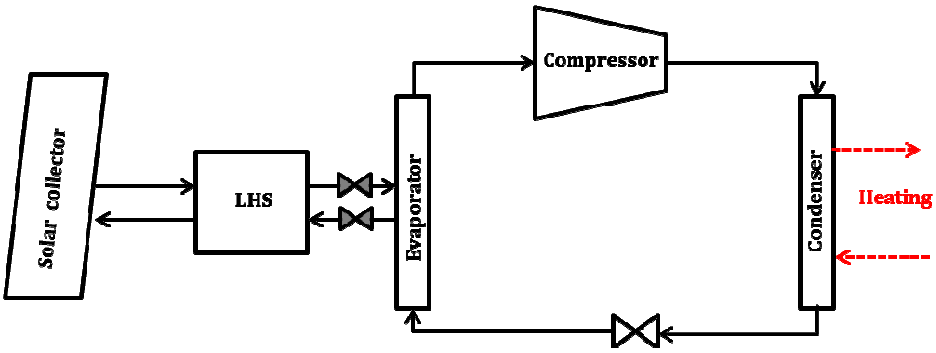

Figure 1.6 The heating cycle for vapor compression system

In the hot season when there is a need for cooling the building, the LHS is disconnected from the evaporator by valves. And the VC air conditioning system cools the building as it was mentioned before. The hot water which comes from the latent heat storage will be used for domestic hot water, Figure 1.7. In this system, the compressor operates with grid electricity.

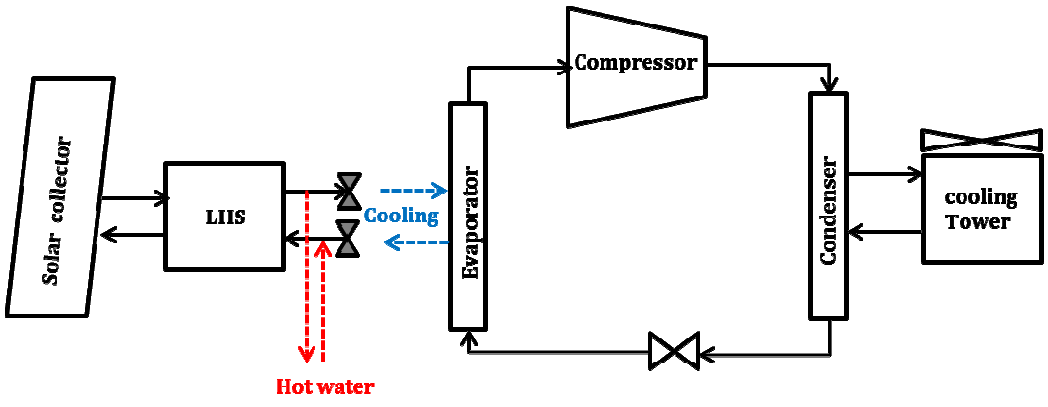

Figure 1.7 The cooling cycle for a vapor compression cycle

Case2: Integrated VC system integrated with solar thermal collector, LHS and PV panels

The system principle is the same as in the previous case. In this case the compressor gets its power from PV panels and the cooling water for the condenser comes from cooling tower. The primary energy consumption of the building is all renewable. One of the benefits of the system is that when the air conditioning system in not in operation, the delivered electricity from the PV panels can be used for domestic lighting or it can be stored. The supply hot water temperature for driving the VC system is in the range of 20 -40 ^{o}C.

1.5.2 Single effect solar absorption system

As it is shown in Figure 1.8 the solar energy is gained through the solar collector and is accumulated in the thermal storage. The hot water from hot storage is supplied to the generator to boil off water vapor from the solution of lithium bromide – water. The water vapor is cooled down in the condenser and then passed to the evaporator where it is again evaporated at lower pressure and temperature. The strong solution leaving the generator and flowing to the absorber passes the solution heat exchanger to preheat the weak solution entering the generator. In the absorber the strong solution absorbs the water vapor leaving the evaporator.

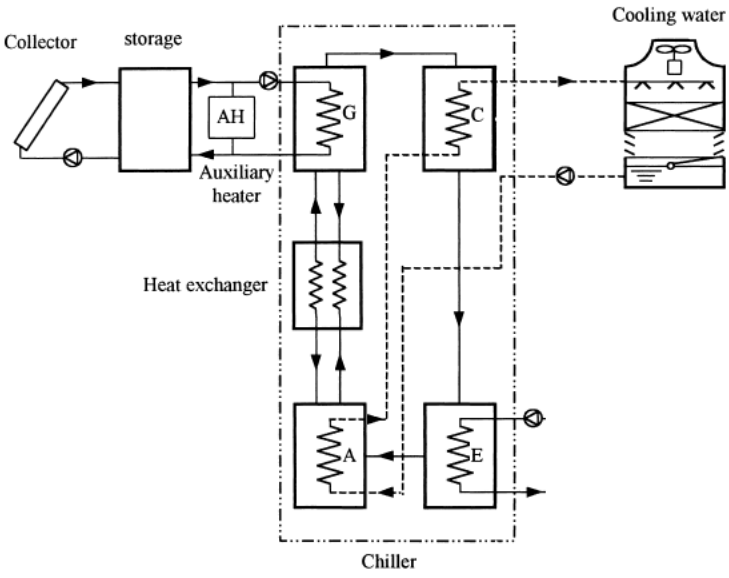

Figure 1.8 Absorption air conditioning system
G: Generator, A: Absorber, C: Condenser, E: Evaporator

An auxiliary heater is provided that when the temperature of hot water which is supplied to the system is not sufficient to drive the generator, the water will be heated to the required temperature level needed by the generator.

Due to the volatile energy prices and environmental concerns, absorption heat pumps have received a lot of attention. Despite the low coefficient of performance of absorption systems in comparison to vapor compression systems, absorption systems are environmentally friendly since the working fluids for these systems do not cause ozone depletion.

The main advantage of absorption systems is that the amount of electricity to drive the system is only limited to the solution pump that does not consume that much electricity in compression to vapor compression systems.
The cooling coefficient of performance of the absorption system is defined as the heat load in the evaporator per unit of heat load in the generator and can be written as (Herold *et al.*, 1996):

$$COP_{cool} = \frac{Q_e}{Q_g + W_p} \quad \textbf{(1.3)}$$

The heating COP of the absorption system is the ratio of the combined heating capacity, obtained from the absorber and condenser, to the heat added to the generator and can be written as (Herold *et al.*, 1996):

$$COP_{heat} = \frac{Q_a + Q_c}{Q_g + W_p} \quad \textbf{(1.4)}$$

Neglecting the pump power, the COP of heating can be also written as:

$$COP_{heat} = \frac{Q_e + Q_g}{Q_g} = 1 + COP_{cool} \quad \textbf{(1.5)}$$

So the COP of heating is in all cases greater than the cooling COP.
Many parameters such as the temperature and flow rate of chilled, cooling and hot water effect the performance of absorption systems and several studies have been done on it. Bakhtiari et al. have done experimental and numerical analysis on H_2O- LiBr absorption heat pumps, with cooling capacity of 14 kW and heating capacity of 33 kW (Bakhtiari *et al.*, 2010).
Gomri investigated the potential of single and multi-effect absorption systems and obtained similar results as Bakhtiari et al. He showed that for each condenser and evaporator temperature, there is an optimum generator temperature. At this point the COP and exergetic efficiency of the systems become maxima (Gomri, 2010). The minimum temperature requirement to power the single effect LiBr/ water absorption system has been investigated by Li and Sumathy and a temperature in the range of 70-85^{o}C was obtained (Li and Sumathy, 2000). Balaras et al. indicated that the single-effect system gives best results in the temperature range 80–100 ^{O}C. The average COP of the absorption cooling system is in the range of 0.6 – 0.8 (Balaras *et al.*, 2007).

Performance of an absorption system is also dependent on the chemical and thermodynamic properties of the working fluid. The two common working fluids are LiBr/ water and Ammonia/ water. Wilbur and Manchini compared the coefficient performance of absorption systems with different working fluids (Wilbur and Manchini, 1976).

Their studies show that the LiBr/ water systems have higher COP than systems with other working fluids. Li and Sumathy (Li and Sumathy, 2000) characterized the main disadvantages of Ammonia/ Water system as follows:

- The coefficient of performance for the Ammonia/ Water system is lower than for LiBr/ Water.
- LiBr/ Water absorption units require lower generator inlet temperature (77 -88 ^{o} C) than Ammonia/ water units (90 – 180 ^{o}C).
- There is limitations on utilizing ammonia- water units because of the hazards associated with the use of ammonia.
- The Ammonia/ water absorption system requires higher pressure and hence higher pumping power.
- A Rectifier is required in this system to separate ammonia and water vapor at the generator outlet.

For these reasons the lithium bromide – water system is considered to be better suited for this solar absorption system.

Case 3: Solar absorption system with LHS and ATES

The principle working of the system is the same as it was mentioned before. In this system instead of water storage, a LHSU will be implemented in the system and an Aquifer Thermal Energy Storage (ATES) will be applied instead of a cooling tower.

ATES stores thermal energy is an aquifer (natural groundwater basin). Two groups of wells, which are hydraulically coupled and separated by a suitable distance, are used for this purpose. Around one of the well group's cold can be stored and around the other heat can be stored. In the basic concept groundwater is pumped from one of the well groups, and then heated or cooled within the cooling/ heating system before being re-injected back into the aquifer in the other well group.

In the absorption cooling cycle the refrigerant extracts heat from the chilled water which comes from the building in the evaporator. The low temperature and pressure refrigerant vapor will flow to the absorber. Simultaneously, the condenser and absorber are connected to the ATES. So from the cold well the water with the temperature in range of 7-9 ^{o} C flows through the heat exchanger to cool the water which flows in to the absorber and condenser and then the hot water from heat exchanger flows in to the warm water well, Figure 1.9.

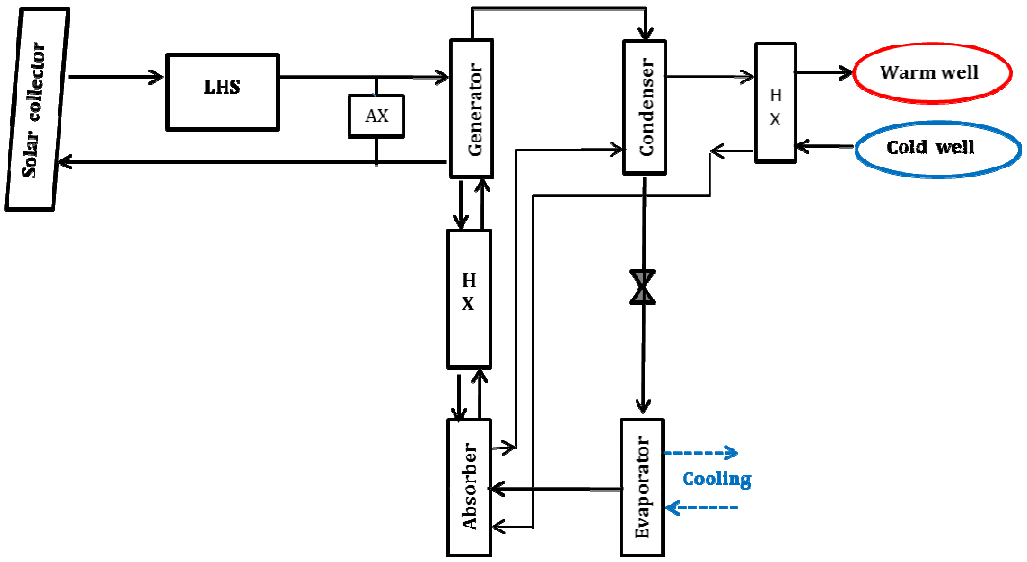

Figure 1.9 Solar absorption cooling cycle

For the heating cycle, the hot water from LHS flows to the generator. The cooling water from building flows through the absorber and condenser. The hot water within the temperature range of 13- 15 ^{O}C from warm water well flows through the heat exchanger and heats the water in the evaporator coils.

The cold water well will be loaded with the cold water which flows out of evaporator, Figure 1.10. In this system an auxiliary heater is implemented so that when the inlet hot water temperature is lower than the required temperature, the water will be heated in the auxiliary heater.

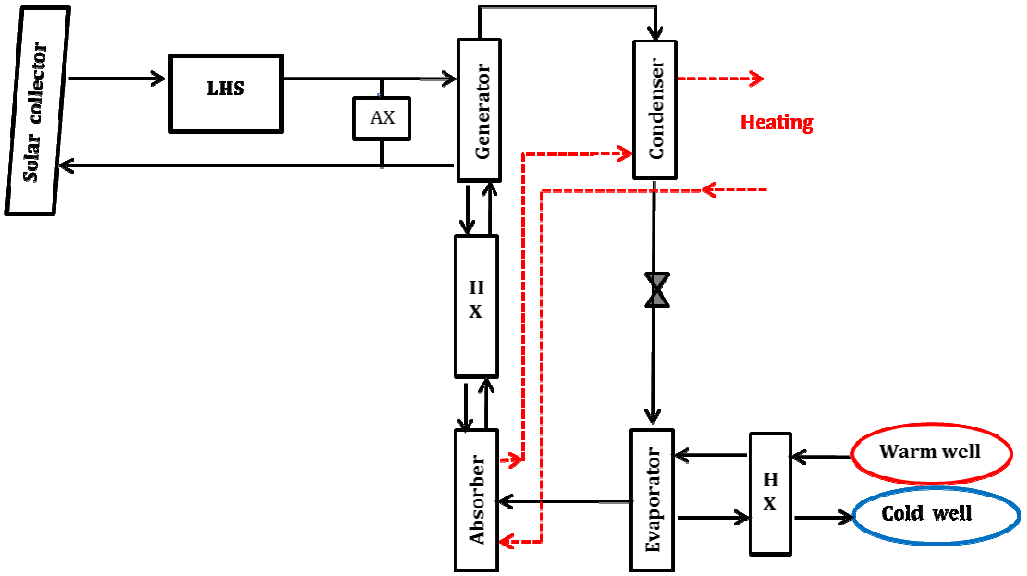

Figure 1.10 The heating cycle of absorption system

Case 4: Solar absorption system with LHS

The cooling cycle of the system is similar to the case 3. Instead of an ATES a cooling tower is implemented in this system, Figure 1.11. Lof and Tybout (1974) analyzed this system for eight cities in USA and studied the system from economical point of view. For the heating cycle, the absorption system will be disconnected. The hot water for heating the building will be directly obtained from the solar collector and latent heat storage, Figure 1.12.

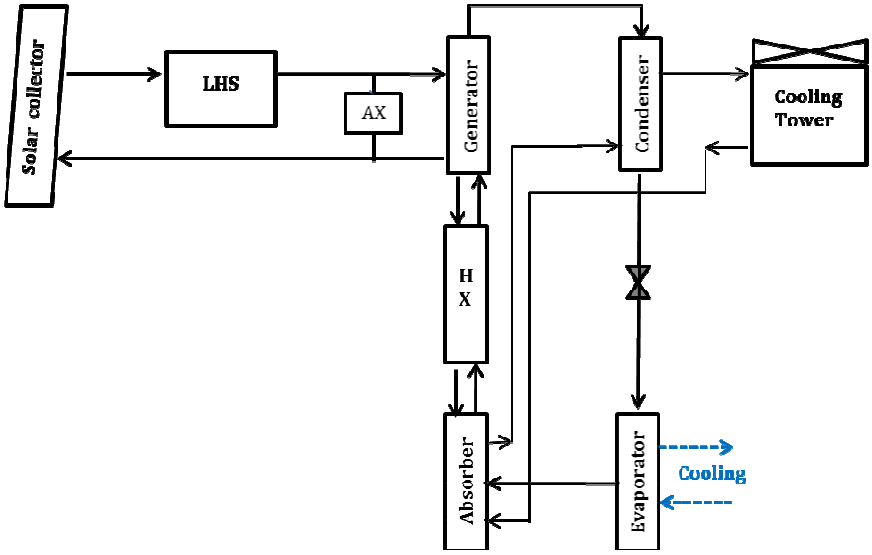

Figure 1.11 The cooling cycle for case 4

The disadvantages of this case are that there is large investment on the absorption system which is not going to be used during the winter. Also applying a cooling tower is not possible for everywhere and there are some problems with water consumption, water make-up and cleaning, formation of fog, and the risk of Legionella bacteria growth (Helm *et al.*, 2009).

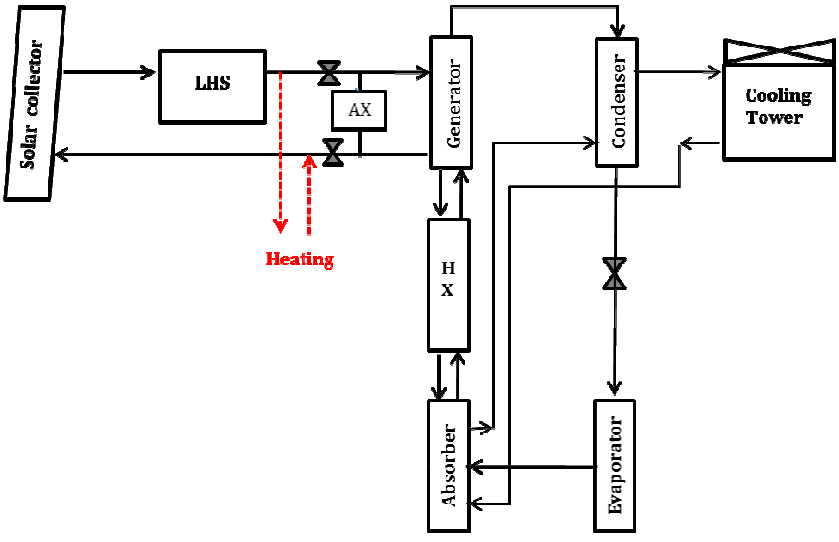

Figure 1.12 The heating cycle for case 4

1.6 Solar Thermal Collector

As it was mentioned in the previous section the driving inlet hot water temperature for both cases 1 and 2 is around 20-40 ^{o} C, so the solar collector should provide temperature around 40-55 ^{o} C. The average inlet generator temperature for absorption in cases 3 and 4 is between 75-90 ^{O} C, so the solar collector should provide temperature higher than 90 -105 ^{O} C. As it is shown in Table 1.2 flat plate solar collectors could provide the desired water temperature for driving the vapor compression system and evacuated tube collectors are suitable for driving the absorption systems.

Table 1.2 Thermal Solar Collector Types (Kalogirou, 2004)

Collector type	Absorber type	Concentration ratio	Indicative temperature range (^{o} C)
Flat plate	Flat	1	30-80
Evacuated tube	Flat	1	50-200
Compound parabolic	Tubular	1-5	60-240

Note: Concentration ratio is the aperture area divided by receiver/ absorber area.

In solar thermal collectors the efficiency of the collector is dependent on the ambient temperature, the mean collector temperature and solar radiation.

$$\eta = \eta_0 - a_1 \frac{T_m - T_{amb}}{G_\perp} - a_2 \frac{(T_m - T_{amb})^2}{G_\perp} \qquad \textbf{(1.6)}$$

η_0 is a conversion factor and a_1 and a_2 are the loss coefficients, which are taken from the manufacturers data. As it is shown in Figures 1.13 and 1.14, the efficiency of solar collectors decreases as the x value ($\frac{T_m - T_{amb}}{G_\perp}$) increases.

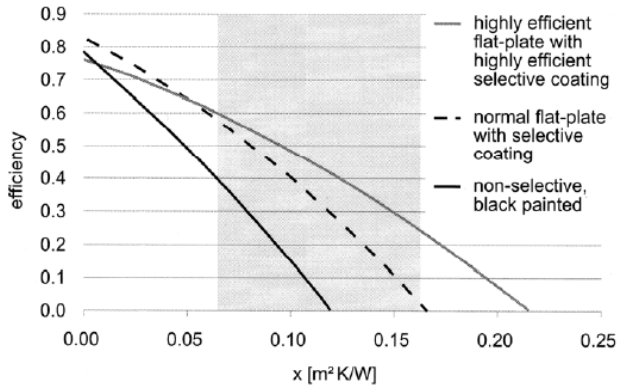

Figure 1.13 Efficiency curve for different type of flat plate solar collector (Henning, 2007)

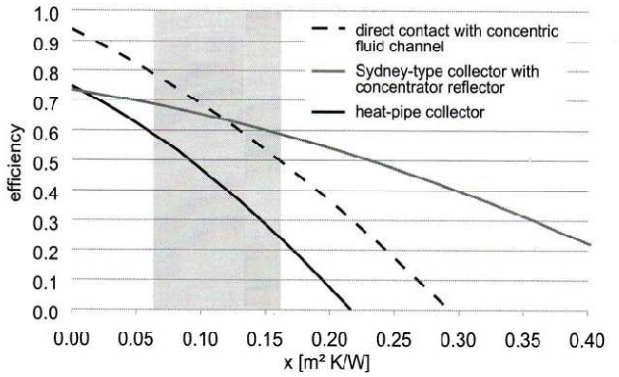

Figure 1.14 Efficiency curves for typical evacuated tube collectors (Henning, 2007)

1.7 System Selection

As it was mentioned in section 1.4 , because the building is a waiting room, the cooling load of the building is much higher than the heating load so that the selection of the system will be based on the cooling demand.
As it is shown in Table 1.3, the COP of the vapor compression system is much higher than the absorption system. On the other hand, the supply hot water temperature for driving the absorption system is much higher than for the vapor compression system which results in utilizing evacuated tube solar collector that can heat the water around 90- 105 ^{o} C. The provided maximum hot water temperature from flat plate solar collector is around 80 ^{O}C, which is sufficient for driving vapor compression systems.

Table 1.3 Characteristic of different vapour compression and absorption systems

System	Vapour compression	Absorption
COP	3-5	0.6-0.8
Supply hot water temperature	20-40 ^{o}C	70-90 ^{o}C
Refrigerant	R134	Water
Solar thermal collector	Flat plate	Evacuated tube
Solar thermal collector price	250 €/m^2	700 €/m^2
PV panels price [a]	5 €/w_P	-
Chiller price	200 €/ kW [a] $_{cooling}$	250 €/ kW [b] $_{cooling}$

[a] (Kim and Infante Ferreira, 2008)
[b] (Mokhtar et al, 2010)

The required solar collector area is a function of efficiency of solar collector, the output power of solar collector and the solar radiation:

$$A = \frac{\dot{Q}_{solar}}{\eta_{collector} * G_{\perp}} \quad \textbf{(1.7)}$$

The approximate solar collector area is shown in Table 1.4. It is assumed that the flat plate and evacuated tube solar collectors have 60% efficiency and the PV panels have 10% efficiency. Based on evaporating temperature around 3 ^{o} C and condensing temperature 40 ^{o} C and the second law efficiency ratio of 0.45 the COP of the vapor compression is considered as 4. For the absorption system with the heat supply temperature is 85 ^{o} C and the second law efficiency ratio of 0.6 the COP of the system calculated as 0.7. The maximum solar radiation is considered 500 and 800 W/m^2 for winter and summer, respectively.

Table 1.4 Approximate solar collector area for different cases (m^2)

	Flat plate collector	Evacuated tube collector
Case 1	100	-
Case2	100	-
Case 3	-	215
Case 4	-	215

Table 1.5 Estimation of systems capital cost in €

	PV panels	Flat plate collector	Evacuated tube	Chiller	total
Case 1	-	25,000	-	14,400	39,400
Case2	90,000	25,000	-	14,400	129,400
Case 3	-	-	150,000	18,800	168,800
Case 4	-	-	150,000	18,800	168,800

The capital cost estimation of different cases is shown in Table 1.5. Case 1 has the lowest capital cost investment but the operating cost is higher than other cases because of driving the compressor which also increases the maintenance cost. The life time of the vapor compression system is around 8 years which is half of the single effect absorption system life time (Elsafty and Al-Daini, 2002). In the Netherland the electricity price is 0.22 €/ kWh (CBS, 2007). Assuming the total working hours of the vapor compression system, during 16 years for 5 months and each day for 8 hours, as 192000 hours with the power of 18 kW the total operating cost will be 76,032 €. In which the price of the chiller for the second 8 years must be added to the total price of the system. So in total the operating cost and the capital cost of case 1 for 16 years will be 130,000. In this estimation the maintenance cost of the vapor compression system is not considered which increases the cost of the system due to the compressor. On the other hand the system is not environmental friendly since it needs to import electricity from the grid.

Case 2 seems to be a good solution but the price of inverter (DC/ AC conversion) was not considered in the estimation and as it was mentioned before the solar absorption is more environmentally friendly since the working fluid in this system does not cause ozone depletion. Due to the compressor the system maintenance cost is higher than the absorption system.

For case 3, since in the Schiphol airport an ATES is already available, there is no need to invest in it and the electricity consumption and the operating cost of the system is much lower than for case 1 (Riffat and Qiu, 2004), and the life time of the absorption system is around 16 years. The maintenance cost of absorption system is much lower than vapor compression system. As it was discussed before in case 4 the absorption system will be used only for cooling during the hot season and in the winter it is not going to operate so from economical point of view this system is not beneficial.

1.8 PCM Selection

The selection of an appropriate PCM requires the PCM to have a melting temperature within the practical range of application; so the selection was dictated by the temperature required for efficient operation of the hot side of the absorption air conditioning system.
Since LiBr/water absorption systems operate with generator temperatures in the range of 75-90 ^{o} C, the PCM melting temperature should be higher than the inlet generator temperature. Among the different PCMs which were summarized by Sharma et al., Kenisarin and Mahkamov and Zalba et al.(Zalba et al., 2003; Kenisarin and Mahkamov, 2007; Sharma et al., 2009) some PCMs are selected for application in the system, which are shown in Tables 1.6 and 1.7.

Table 1.6 Selected PCMs for application in solar LiBr/ water absorption systems with melting temperature in range of 100- 150 ^{o}C

Heat storage material	Type	Melting point (^{o}C)	Heat of Fusion (kJ/kg)
Methyl fumarate	Organic (fatty acid)	102	242
$MgCl_2$. $6H_2O$	Inorganic	115	165
Erythritol	Organic	118	339.8
HDEP	Organic	100- 150	200
RT 110	Organic(Paraffin)	112	213
Acetanilide	Organic(non-Paraffin)	118.9	222
Succinic anhydride	Organic(non-Paraffin)	119	204

Table 1.7 Selected PCMs for applications in solar LiBr/ water absorption system with melting temperature in range of 79- 96^{o}C

Heat storage material	Type	Melting point (^{o}C)	Heat of Fusion (kJ/kg)
Acetamid	Organic (fatty acid)	81	241
Mg $(NO_3)_2$. $6H_2O$	Inorganic (Salt hydrates)	90	167
KAl $(So_4)_2$. 12 H_2O	Inorganic (Salt hydrates)	91	184
RT 90	Organic (Paraffin)	90	197
RT 80	Organic(Paraffin)	79	209
Naphthalene	Organic(non-Paraffin)	80	147.7
Alpha naphtol	Organic(non-Paraffin)	96	163

Among the PCMs presented in Tables 1.6 and 1.7 Erythritol has the highest latent heat of fusion. Erythritol is a sweetening agent and is used for drinks in order to sweeten without adding calories. Kakiuchi et al. (1998) investigated the thermo- physical properties of Erythritol. Erythritol has a high heat of fusion, almost equal to ice. In Erythritol, the biggest problem is the volume change during the phase change of solid to liquid which changes about 10% during solid to liquid phase transition. So, a heat exchanger is required with a structure or special method which allows for volume change (Kakiuchi et al., 1998). The enthalpy curve of Erythritol is shown in Figure 1.15.

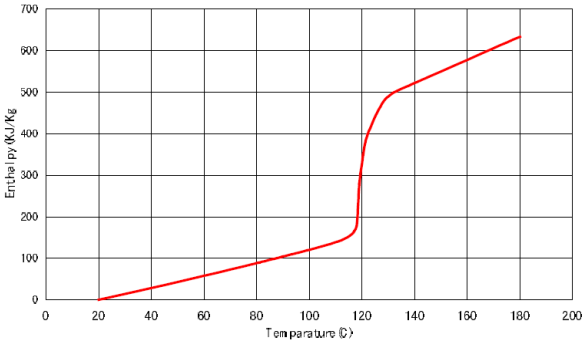

Figure 1.15 The Enthalpy curve of Erythritol

The energy storage capacity of Erythritol is 20% higher than magnesium chloride hexahydrate (MCHH) and 32% more higher RT100. The high energy density of Erythritol combined with the fact that it is commercially available makes Erythritol suitable to be considered as energy storage material (Agyenim *et al.*, 2007).

1.9 Research objective

The main goal of this thesis is to identify the potential of phase change materials as a latent heat storage to contribute with solar assisted single effect absorption cooling system for a specified building in the Netherlands. In this research the system design regarding to the cooling load of the specified building and analysis the behavior of the system during the charging and discharging process of latent heat storage unit will be studied.

1.10 Problem approach

After through literature research and defining the objective of the research, a method for approaching the solution has been developed. The latent heat storage unit should provide the hot water for driving the absorption air conditioning system. Therefore, as a first step in Chapter 2, mathematical model for the absorption system based on mass and energy balances and heat transfer equations will be developed. The model will be implemented in MATLAB software and the numerical results will be validated with results from the literature.
Chapter 3 will be devoted to developing mathematical model for the latent heat storage unit based on the energy balances and heat transfer equations. Same as the absorption system, the model will be implemented in MATLAB software and the results will be validated with the experimental results from the literature.
Regarding to the maximum cooling load of the mentioned building in section 1.4, the single effect absorption system and the latent heat storage unit will be designed and the behavior of the systems to the control parameters will be investigated in Chapter 4. In this chapter, charging and discharging process of latent heat storage integrated with solar collector field and the absorption cooling system will be studied. Chapter 5, is devoted to conclusions and recommendations for the future work.

Chapter 2

Absorption system

2.1 Introduction

Absorption heat pumps supplied with waste energy and water heated through solar collectors have received a lot of attention due to the high energy prices and environmental concerns. Many investigations have been done on single effect absorption systems (Ng *et al.*, 1994; Joudi and Lafta, 2001; Florides *et al.*, 2003). Several studies investigated the effect of different parameters on the performance of absorption heat pumps (Lorton *et al.*, 2000; Lee and Sherif, 2001; Bakhtiari *et al.*, 2010). Different mathematical models of various complexity have been developed for different purposes, such as simulation of absorption system, optimization and design (Joudi and Lafta, 2001; Cascales *et al.*, 2010).

In order to characterize the performance of the absorption system, a mathematical model for the absorption system is developed in this chapter. For each component, mathematical models are developed based on energy and mass balances. In the first section the analytical model for steady state LiBr- H_2O absorption system is developed and the simulation results are validated with the experimental results.

As it was explained before the absorption system consists of five basic components, an absorber, a generator, a condenser, an evaporator and a solution heat exchanger as shown in Figure 2.1.

A solution heat exchanger, placed between the absorber and the generator, makes the process more efficient. Low pressure water vapor is absorbed in the absorber by the solution. The heat generated during the absorption is removed by the cooling water.

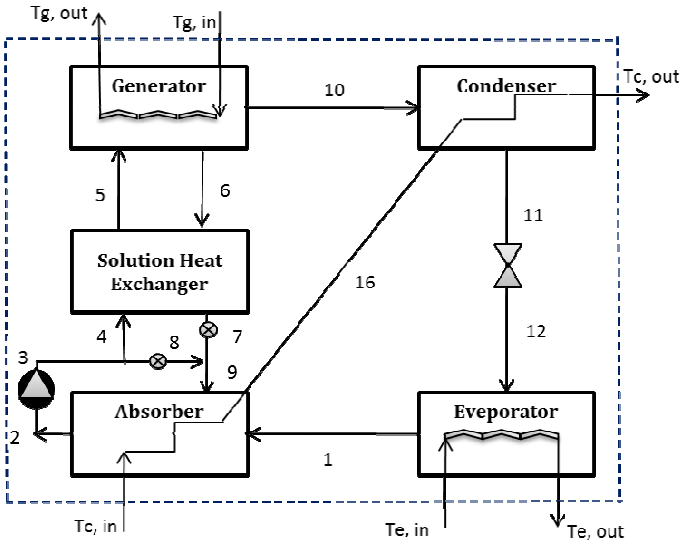

Figure 2.1. Schematic diagram of the simulated absorption system

A pump circulates the weak solution; with a part of it being sent to the generator through the solution heat exchanger. In the generator, the weak solution which comes from the solution heat exchanger is heated to boil and release water vapor.
The strong solution with LiBr is returned to the solution heat exchanger and absorber. The water vapor is condensed to liquid in the condenser, and then it is passed via an expansion valve to the evaporator.

2.2 Mathematical model

For developing the analytical model for simulating the LiBr- H_2O absorption system, each component of the absorption system is treated as a control volume with its own inputs and outputs. The mathematical model is described by mass balances, energy balances and heat transfer equations between the internal and external streams for each component.
Several assumptions and hypothesis are considered for the systems which are as follows:

- The pressure drop in the pipes and vessels is negligible.
- The heat losses from the generator to the surroundings and the heat gains to the evaporator from the surroundings are negligible.
- The expansion process of the expansion device is at constant enthalpy.
- The water at the outlet of evaporator is saturated vapor.
- The water at the outlet of condenser is saturated liquid.
- The water vapor at the outlet of generator is superheated.
- The mass accumulation in the generator, absorber, condenser, evaporator and the solution heat exchanger is neglected.

The empirical equations of enthalpies, temperatures, concentrations and vapor pressures of the LiBr- H_2O given by the ASHRAE are used which are presented in Appendix A (ASHRAE, 2009).

I. Absorber

In the absorber, the water vapor comes from the evaporator, is absorbed by the strong LiBr solution which comes from the solution heat exchanger, the heat generated during absorption is rejected to a water flow. The weak LiBr solution is pumped through the solution heat exchanger.

Conservation equations

- Mass conservation:

$$f_2 = f_3 \quad \textbf{(2.1)}$$

$$f_1 + f_9 = f_2 \quad \textbf{(2.2)}$$

- Conservation of absorbate:

$$f_9 X_9 = f_2 X_2 \quad \textbf{(2.3)}$$

- Energy balance:

$$Q_a = -f_2\, h_2\,(X_2, T_2) + f_1\, h_1\,(q_v, T_e) + f_9\, h_9\,(X_9, T_9) \quad \textbf{(2.4)}$$

$$Q_a = f_c\, C_{pc}\,(T_{16} - T_{c,in}) \quad \textbf{(2.5)}$$

Constitutive equations

$$Q_a = U_a\, A_a\, \Delta T_{LMa} \quad \textbf{(2.6)}$$

The logarithmic mean temperature of the absorber is estimated with an approximated equation (Bakhtiari *et al.*, 2010) is given by:

$$\Delta T_{LMa} = \frac{(T_9 - T_{16}) - (T_2 - T_{c,in})}{ln\,\frac{(T_9 - T_{16})}{(T_2 - T_{c,in})}} \quad \textbf{(2.7)}$$

II. Solution heat pump circuit

The weak LiBr-H_2O solution which comes from the absorber flows through the pump. It is assumed that half of the solution enters the solution heat exchanger and half of it mixes with the strong solution that comes from the solution heat exchanger (Joudi and Lafta, 2001).

Conservation equations

- Mass conservation

$$f_2 = f_3 = 2f_4 = 2f_8 = f_a \quad \textbf{(2.8)}$$

$$f_6 = f_7 \quad \textbf{(2.9)}$$

$$f_8 + f_7 = f_9 \quad \textbf{(2.10)}$$

- Conservation of absorbate

$$f_2 \mathrm{X}_2 = f_3 \mathrm{X}_3 \quad \textbf{(2.11)}$$

From equation 2. 8:

$$X_2 = X_3 = X_a \quad \textbf{(2.12)}$$

$$f_3 X_3 = f_4 X_4 + f_8 X_8 \quad \textbf{(2.13)}$$

Substituting equation 2.8 in equation 2.13 and eliminating f_3 provides:

$$X_3 = X_4 = X_8 = X_a \quad \textbf{(2.14)}$$

$$f_9 X_9 = f_8 X_8 + f_7 X_7 \quad \textbf{(2.15)}$$

Substituting equation 2.8 and 2.14 into 2.15 gives

$$X_9 = \frac{1}{2}\frac{f_2}{f_9} X_2 + \frac{f_7}{f_9} X_7 \quad \textbf{(2.16)}$$

- Energy balance

The pump power is calculated by:

$$W_p = \frac{f_2}{\rho_2}\frac{(P_c - P_e)}{\eta_p} \quad \textbf{(2.17)}$$

❖ The density of the LiBr concentration is calculated by the given equation in Appendix A (Lee *et al.*, 1990).

III. Solution Heat Exchanger

In the solution heat exchanger the strong LiBr solution which comes from the generator exchanges heat with the weak LiBr solution.

Constitutive equations

$$T_4 = T_2 \quad \textbf{(2.18)}$$

$$\varepsilon = \frac{T_{6-}T_7}{T_{6-}T_4} \quad \textbf{(2.19)}$$

$$T_7 = T_{6-}\varepsilon(T_{6-}T_4) \quad \textbf{(2.20)}$$

❖ It is assumed that there is no boiling in the heat exchanger so that the specific heat capacity can be assumed to be constant.

Conservation equations

- Mass conservation

$$f_5 = f_4 = \frac{1}{2} f_2 \quad \textbf{(2.21)}$$

$$f_7 = f_6 \quad \textbf{(2.22)}$$

- Energy balance

$$f_4\, C_{P4}(T_5 - T_4) = f_6\, C_{P6}(T_6 - T_7) \quad \textbf{(2.23)}$$

$$T_5 = \frac{f_6\, C_{P6}}{f_4\, C_{P4}}(T_6 - T_7) + T_4 \quad \textbf{(2.24)}$$

❖ The specific heat of LiBr solution is obtained by the given equation in Appendix A (ASHRAE, 2009).

IV. Generator

In the generator the external hot fluid provides the heat to boil the solution, super-heated refrigerant, which separates from the solution, is generated and flows to the condenser. The strong solution enters through the solution heat exchanger to preheat the weak solution.

Conservation equations

- Mass conservation

$$f_1 = f_{10} \quad \textbf{(2.25)}$$
$$f_5 - f_1 = f_6 \quad \textbf{(2.26)}$$

- Conservation of absorbate

$$f_5\, \mathrm{X}_5 = f_6\, \mathrm{X}_6 \quad \textbf{(2.27)}$$
$$X_6 = X_g = \frac{f_5\, X_5}{f_6} \quad \textbf{(2.28)}$$

- Equilibrium equation

$$T_6 = T_g = F(T_c\,, X_6) \quad \textbf{(2.29)}$$

- Energy balance:

$$Q_g = f_g\, C_{pg}\,(T_{g,in} - T_{g,out}\,) \quad \textbf{(2.30)}$$
$$Q_g = f_6\, h_6\,(X_6, T_6) + f_1 h_{10}(P_c, T_5, T_c) - f_5 h_5(X_5, T_5) \quad \textbf{(2.31)}$$

Constitutive equations

$$Q_g = U_g\, A_g\, \Delta T_{LMg} \quad \textbf{(2.32)}$$

The approximate equation for calculating the logarithmic mean temperature for the generator is (Bakhtiari *et al.*, 2010) given by:

$$\Delta T_{LMg} = \frac{(T_{g,in} - T_6) - (T_{g,out} - T_5)}{ln\ \frac{(T_{g,in} - T_6)}{(T_{g,out} - T_5)}} \quad \textbf{(2.33)}$$

V. Condenser

In the condenser the superheated vapor is cooled down and condensed to saturated liquid with the cooling water which comes from the absorber.

Conservation equations

- Mass conservation

$$f_1 = f_{10} = f_{11} \quad \textbf{(2.34)}$$

$$f_{16} = f_c \quad \textbf{(2.35)}$$

- Energy balance

$$Q_c = f_1 \left[h_{10}(P_c, T_5, T_c) - h_{11}(q_l, T_c)\right] \quad \textbf{(2.36)}$$

$$Q_c = f_c \, C_{Pc} \, (T_{c,out} - T_{16}) \quad \textbf{(2.37)}$$

Constitutive equations

$$Q_c = U_c \, A_c \, \Delta T_{LMc} \quad \textbf{(2.38)}$$

In which the Logarithmic mean temperature for the condenser is

$$\Delta T_{LMc} = \frac{\left(T_5 - T_{c,out}\right) - (T_c - T_{16})}{ln \, \frac{\left(T_5 - T_{c,out}\right)}{(T_c - T_{16})}} \quad \textbf{(2.39)}$$

❖ The enthalpy of superheated and saturated liquid water are obtained by the equations given in Appendix A (Mayhew and Rogers, 1994).

VI. Evaporator

In the evaporator the refrigerant evaporates and enters the absorber as a saturated vapor.

Conservation equations

- Mass conservation

$$f_1 = f_{11} = f_{12} \quad \textbf{(2.40)}$$

$$f_{13} = f_e \quad \textbf{(2.41)}$$

- Energy balance

$$Q_e = f_1 \left[h_v(q_v, T_e) - h_l(q_l, T_c)\right] \quad \textbf{(2.42)}$$

$$Q_e = f_e \, C_{Pe}(T_{e,in} - T_{e,out}) \quad \textbf{(2.43)}$$

Constitutive equations

$$\mathrm{Q_e} = U_e\, A_e\, \Delta \mathrm{T_{LMe}} \quad \textbf{(2.44)}$$

In which the Logarithmic mean temperature for the evaporator is

$$\Delta T_{LMe} = \frac{(T_{e,in} - T_e) - (T_{e,out} - T_e)}{ln\,\frac{(T_{e,in} - T_e)}{(T_{e,out} - T_e)}} \quad \textbf{(2.45)}$$

The overall energy balance equation for the whole absorption cycle is given by

$$Q_e + Q_g - Q_a - Q_c + W_p = 0 \quad \textbf{(2.46)}$$

The flow diagram of the system is shown in Figure 2.2. The blue dashed line shows the system boundary. The absorber, solution heat exchanger and the heat pump circuits are shown as separate components in the flow diagram. For each component the inputs and outputs are shown.

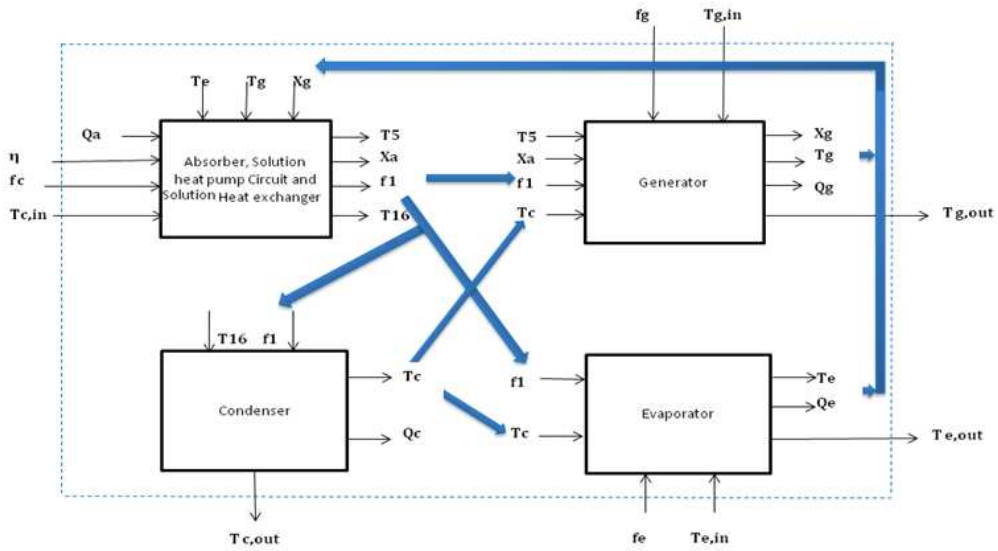

Figure 2.2 Flow diagram of absorption system

The COP for the system is defined as

$$COP_{cool} = \frac{Q_e}{Q_g + W_p} \quad \textbf{(2.47)}$$

$$COP_{heat} = \frac{Q_a + Q_c}{Q_g + W_p} \quad \textbf{(2.48)}$$

2.3 Implantation of the model in MATLAB/ SIMULINK

The developed mathematical model for single effect absorption system is implemented in MATLAB/ SIMULINK. For each component a MATLAB function is written in SIMULINK in which the developed mathematical equation are implemented in. The MATLAB codes for each component are given in Appendix B.

2.4 Validation of the absorption system

The quantitative validation is done by comparing the simulation results with the results from Jeong and Garimella (2002). The input values and design parameters are shown in Tables 2.1 and 2.2 .

Table 2.1 Input values for simulated absorption system

Inputs	description	Unit	value
f_g	Hot water mass flow rate	kg/s	14.1
$T_{g,in}$	Hot water input temperature	^oC	85
f_c	Cooling water mass flow rate	kg/s	20.1
$T_{c,in}$	Cooling water input temperature	^oC	30
f_e	Chilled water mass flow rate	kg/s	10.08
$T_{e,in}$	Chilled water input temperature	^oC	12
f_3	Solution mass flow rate	kg/s	8.03

Table 2.2 Parameters values for simulated absorption system

Parameters	description	Unit	value
UA_g	Conductance of generator coils	kW/K	24.30
UA_a	Conductance of absorber coils	kW/K	98.28
UA_c	Conductance of condenser coils	kW/K	17
UA_e	Conductance of evaporator coils	kW/K	53.17
η_p	Pump efficiency	%	60
ε	Heat transfer effectiveness		0.85

The simulation and experimental results are given in Table 2.3. As it can be observed there is a good agreement between simulation results and experimental results. The absorption cycle is shown in a temperature- pressure diagram of LiBr- water in Figure 2.3.

Table 2.3 Results comparison with Ref (Jeong and Garimella, 2002)

Variable	Description	Simulation results	Experimental results	Unit	Δ%
f_1	Mass flow rate of refrigerant	0.089	0.086	Kg/s	3.48
X_2	Output concentration of Li/Br in the absorber	54.8	54.4	%	0.73
X_6	Output concentration of Li/Br in the generator	56.04	55.8	%	0.43
T_5	Output temperature of Li/Br from solution pump	66.95	65.1	^oC	2.84
T_2	Output temperature of Li/Br in the absorber	34.17	33.8	^oC	1.09
T_7	Output temperature of strong Li/Br solution at the solution heat exchanger	40.18	39.6	^oC	1.46
$T_{g,out}$	Output temperature of hot water	80.05	80.7	^oC	-0.81
$T_{c,out}$	Output temperature of cooling water	35.96	35.7	^oC	0.73
$T_{e,out}$	Output temperature of chilled water	7.25	8.0	^oC	-9.37
Q_e	Load of evaporator	209.6	209.6	kW	0
COP		0.71	0.70		1.42

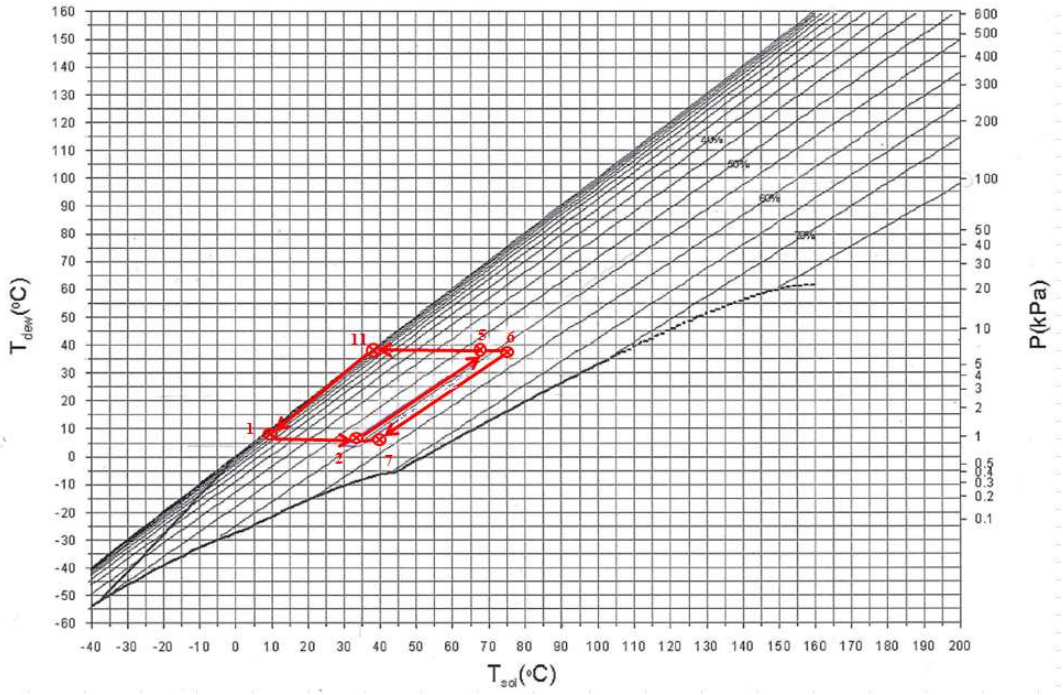

Figure 2.3 The temperature – pressure diagram of absorption cycle

As it is shown in the figure, the difference between the week solution and strong solution of LiBr concentration is just 1.4% , which is really low. This difference is due to the low solution mass flow rate.

2.5 Conclusion

In this chapter simplified model for single effect absorption cooling system based on mass, energy balances and heat transfer equations was developed. Mathematical model was implemented in MATLAB/ SIMULINK software. The results were validated with the results from the literature and a good agreement was observed.

Chapter 3

Latent Heat Storage

3.1 Introduction

The study of the heat transfer characteristics of melting and solidification processes is one interesting research area in which lots of studies have been developed (Lazaridis, 1970; Bonacina *et al.*, 1973; Costa *et al.*, 1991; Lacroix, 1993). The analysis of heat transfer problems during melting and solidification processes is called Stefan problem. Predicting the behavior of phase change systems is difficult due to its non-linear nature at moving interface and in addition, two phases have different thermo physical properties.

The Stefan problem was first investigated as pure conduction and later natural convection has been considered during melting and solidification of PCMs (Carslaw and Jaeger, 1959). The different classes of solution available for Stefan problem are numerical and analytical.

Numerical methods, both finite difference (Bonacina *et al.*, 1973) and finite element (Comini *et al.*, 1974) appear powerful in solving the moving boundary problem. The time variant mesh (Yoo and Rubinsky, 1983) approach offers good accuracy but is limited to simple problems and geometries. The fixed mesh approach, in which the latent heat of fusion is usually absorbed into the materials specific heat or enthalpy, is much simpler in practical applications.

As it was mentioned before, the difficulty in solving a phase change problem is the presence of moving boundary in which the heat and mass balance conditions have to be met. One of the methods to solve the moving boundary problem is by enthalpy formulation. In the enthalpy method (Comini *et al.*, 1974; Esen and Ayhan, 1996; Costa *et al.*, 1998), the only unknown is the temperature of the phase change materials and solidification occurs at a uniform temperature. Enthalpy method treats the enthalpy as a temperature dependent variable and constructs the latent heat flow through the volume integration with the use of the enthalpy of the system.

A Respectful numbers of investigations have been done on geometry configuration of the PCM storage (Jones *et al.*, 2006; Vynnycky and Kimura, 2007; Tan, 2008). Vyshak and Jilani (2007) did a comparative study of the total melting time of a phase change material packed in three containers of different geometry configurations, rectangular, cylindrical and cylindrical shell, having the same volume and surface area of heat transfer. They concluded that with the same mass of PCM the cylindrical shell container takes the least time for the same energy storage (Vyshak and Jilani, 2007).
Therefore, in the present study the cylindrical shell container will be considered for the PCM package. In this chapter the problem of phase change will be numerically solved by using finite difference approach and the enthalpy method will be used. The developed model will be validated with the results from literature.

3.2 Mathematical model

The schematic of the latent heat storage unit is shown in Figure 3.1. As it is shown the storage consists of inner tubes and an outer tube. The heat transfer fluid (HTF) and the PCM are separated. The HTF flows through the inner tubes and exchanges heat with the PCM which is located in the outer tube. During the charging process (melting), the hot water which comes from the solar collector exchanges heat with the solid PCM and the PCM starts melting. During the discharging process (solidification), the cold HTF circulates through the inner tube and the PCM exchanges heat with the cold HTF and starts solidifying.

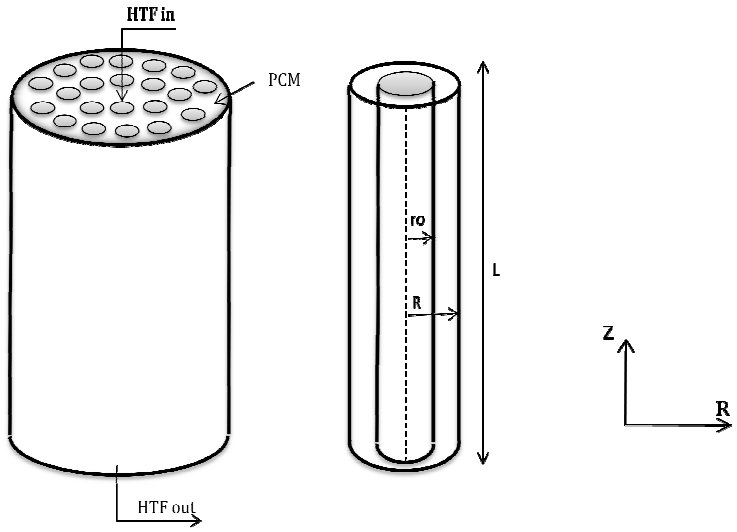

Figure 3.1 Schematic of the latent heat storage unit (the inside radius is r_o and the outside is R)

The theoretical treatment of this problem is similar to that described by (Esen and Ayhan, 1996).
In order to simplify the mathematical model, the following assumptions were made:

- The PCM is homogenous and isotropic (having identical values of a property in all directions).
- The thermal resistance of the inner tube is negligible.

- The thermo physical properties of HTF and PCM are independent of temperature; however the thermal conductivity and the specific heat capacity of the PCM in solid and liquid phase are different.
- The effect of natural convection during melting is neglected.
- The axial conduction in the HTF is negligible.
- The latent heat storage is insulated, so there are no heat losses to the environment.

I. Charging mode

The energy equations for HTF and PCM are expressed as follows:

HTF

$$(\rho C_P)_f \pi {r_o}^2 \frac{\partial T_f}{\partial t} = -(\dot{m} C_P)_f \frac{dT_f}{dz} + \lambda\left(T_{r=r_o} - T_f\right) 2\pi r_o \qquad \textbf{(3.1)}$$

PCM

$$(\rho C_P)_P \frac{\partial T}{\partial t} = div(k_P \; grad \; T) \qquad \textbf{(3.2)}$$

The increase with time of the energy content of an arbitrary volume V is equal to the net heat transfer into V through its surrounding surface area A. So the enthalpy equation is:

$$\frac{d}{dt} \int \rho h \; dV = \int k_p grad T . \bar{n} \; dA \qquad \textbf{(3.3)}$$

where $\bar{n}$ is outward normal to A.

With the enthalpy method it is easy to handle a PCM and its phase change range. The phase change range is introduced as follows (Esen and Ayhan, 1996):

$$h(T) = \begin{cases} C_{p,s} \; T & T < T_{m1} \\ C_{p,l} \; T + \dfrac{\Delta H \; (T - T_{m1})}{\Delta T_m} & T_{m1} \le T \le T_{m2} \\ C_{p,l} \; T + \; \Delta H & T > T_{m2} \end{cases} \qquad \textbf{(3.4)}$$

in which $\Delta T_m = T_{m2} - T_{m1}$.

Initial and boundary conditions:

$$t = o, \quad T_f = T = T_{am} \qquad \textbf{(3.5 a)}$$

$$t > o, \quad T_f(z = 0, r) = T_{f,in} \qquad \textbf{(3.5 b)}$$

$$\frac{\partial T}{\partial z}\,(z = 0, for \; r_0 to \; R) = 0, \quad \frac{\partial T}{\partial z}\,(z = L, for \; r_0 to \; R) = 0 \qquad \textbf{(3.5 c)}$$

$$k \frac{\partial T}{\partial r}\,(z, r = r_o) = \lambda \; (T_{r=r_0} - T_f) \qquad \textbf{(3.5 d)}$$

$$\frac{\partial T}{\partial r}\,(z, r = R) = 0 \qquad \textbf{(3.5 e)}$$

II. Discharging mode

When the heat transfer rate of the PCM to HTF is equal or greater than the heat transfer rate of HTF to PCM the operation mode is changed and the storage unit starts discharging.
For this operating mode, the thermal behavior of the storage unit is governed by the same equations as in the charging mode.

3.3 Numerical simulation

The energy equations 3.1 and 3.2 are integrated in the axial direction z and the (Z, R) plane, respectively. The finite difference equations for HTF and PCM are obtained as follows:
HTF

$$T_{f,j}^{n} = \frac{aT_{r=r_0} + \frac{b}{\Delta z}T_{f,j-1} + \frac{1}{\Delta t}T_{f,j}^{n-1}}{a + \frac{b}{\Delta z} + \frac{1}{\Delta t}} \quad \textbf{(3.6)}$$

where a and b is given by following expressions;

$$a = \frac{2\lambda}{(\rho C_P)_f\, r_o} \quad , \quad b = \frac{\dot{m}_f}{\rho_f \pi r_o^2} \quad \textbf{(3.7)}$$

The energy equation of the HTF, equation 3.6, is discretized using the first order backward finite difference.
The convective heat transfer coefficient depends on the fact that the flow is laminar or turbulent. The Reynolds number expressed as follows:

$$Re_f = \frac{2\dot{m}_f}{\pi N_p \mu_f r_o} \quad \textbf{(3.8)}$$

For laminar flow the Nusselt number is:

$$\boldsymbol{Nu_f} = 3.66 \quad \textbf{(3.9)}$$

and the Gnielinski correlation is applied for the turbulent flow;

$$Nu_f = \frac{\frac{f}{8}\,(Re_f - 1000)\,Pr}{1 + 12.7\,(f/8)^{0.5}\,(Pr^{2/3} - 1)} \qquad 3000 \le Re_f \le 5 \times 10^6 \quad \textbf{(3.10)}$$

where f (Darcy friction factor) is ;

$$f = (0.79\,Ln\,Re - 1.64)^{-2} \quad \textbf{(3.11)}$$

PCM

A fixed control volume element (j, k) is shown in Figure 3.2. As it is shown in the figure the inner radius is R_{k-1} and the outer radius is R_k. Applying the conservation equations on a volume element (j, k) the heat transfer equation is found as follows:

$$\rho V_{j,k}\frac{\partial h}{\partial t} = k_P A_k \frac{\partial T}{\partial R_k} - k_P A_{k-1}\frac{\partial T}{\partial R_{k-1}} + k_P A_j \frac{\partial T}{\partial Z_j} - k_P A_{kj-1}\frac{\partial T}{\partial Z_{j-1}} \quad \textbf{(3.12)}$$

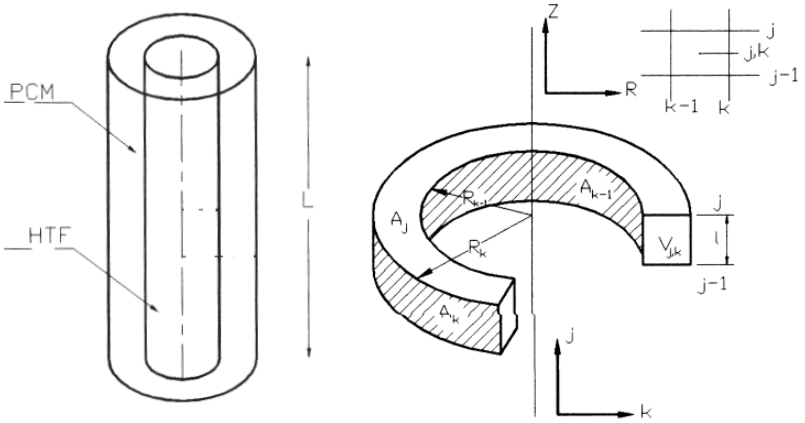

Figure 3.2 Cylindrical control volume element (j, k)(Esen and Ayhan, 1996)

where

$$\frac{\partial T}{\partial R_k} = \frac{T^n_{j,k+1} - T^n_{j,k}}{\Delta R} \quad \textbf{(3.13)}$$

$$\frac{\partial T}{\partial R_{k-1}} = \frac{T^n_{j,k} - T^n_{j,k-1}}{\Delta R} \quad \textbf{(3.14)}$$

$$\frac{\partial T}{\partial Z_j} = \frac{T^n_{j+1,k} - T^n_{j,k}}{\Delta z} \quad \textbf{(3.15)}$$

$$\frac{\partial T}{\partial Z_{j-1}} = \frac{T^n_{j,k} - T^n_{j-1,k}}{\Delta z} \quad \textbf{(3.16)}$$

and

$$\frac{\partial h}{\partial t}_{j,k} = \frac{h^n_{j,k} - h^{n-1}_{j,k}}{\Delta t} \quad \textbf{(3.17)}$$

Substituting the discretized spatial and temporal equations in equation 3.12, the following equation is obtained:

$$(\pi\rho(R_k^2 - R_{k-1}^2)dz\frac{h^n_{j,k} - h^{n-1}_{j,k}}{\Delta t} = \left(2\pi k_P R_k dz\frac{T^n_{j,k+1} - T^n_{j,k}}{\Delta R}\right) - \left(2\pi k_P R_{k-1} dz\frac{T^n_{j,k} - T^n_{j,k-1}}{\Delta R}\right) + \left(\pi k_P (R_k^2 - R_{k-1}^2)\frac{T^n_{j+1,k} - T^n_{j,k}}{\Delta z}\right) - \left(\pi k_P (R_k^2 - R_{k-1}^2)\frac{T^n_{j,k} - T^n_{j-1,k}}{\Delta z}\right) \quad \textbf{(3.18)}$$

The algebraic equation 3.18 should be solved and coupled with equation 3.6 with the boundary conditions which were mentioned previously (3.5 d).

3.4 Validation of the latent heat storage model

The mentioned numerical method has been implemented in a self-written MATLAB computer code that has been designed to resolve the coupled non-linear and time dependent energy equations for HTF and PCM, Appendix C.

The model is validated by the experimental results reported by Agyenim et al (2010). These authors experimentally studied the melting and solidification behavior of Erythritol inside a cylinder with 8 longitudinal fins. The PCM is located in the shell and the HTF flows through the tube. In their study the lower and higher melting temperatures of the Erythritol are given as 115.7 ^{o}C and 119.7 ^{o}C, respectively (Agyenim *et al.*, 2010). The geometry of the shell and tube storage is taken the same as for the experiments; the length of the cylinder and pipe is set to 1m. The outside diameter of the shell is considered 146 mm and the diameter of the pipe though which the HTF flows through is considered as 54 mm. The properties of the PCM and HTF are given in Table 3.1.

Table 3.1 Thermo-physical properties of phase change material (Erythritol)and HTF (Therminol 60)

Property	Value	Unit
Melting point of PCM	117.7	^{o}C
Heat of fusion of PCM	339.8	kJ kg^{-1}
Specific heat of PCM, liquid	2.76	kJ kg^{-1}K^{-1}
Specific heat of PCM, solid	1.38	kJ kg^{-1}K^{-1}
Thermal conductivity of PCM, liquid (140 ^{o}C)	0.326	W m^{-1} K^{-1}
Thermal conductivity of PCM, solid (20 ^{o}C)	0.733	W m^{-1} K^{-1}
Density of PCM, liquid (140 ^{o}C)	1300	Kg m^{-3}
Density of PCM, solid (20 ^{o}C)	1480	Kg m^{-3}
Thermal conductivity of HTF	0.12	W m^{-1} K^{-1}
Specific heat of HTF	1.99	kJ kg^{-1}K^{-1}
Density of HTF	924	Kg m^{-3}
Dynamic viscosity of HTF	10.8*10^{-4}	Pa.s

A HTF mass flow rate of 30 kg/ min and an inlet temperature of 140 ^{o} C were selected for the heat transfer analysis in the system for the charging mode. The initial temperature of HTF and PCM were considered as 80 ^{o} C and 20 ^{o} C, respectively. For the discharging mode, the initial temperature of HTF and PCM are considered as 140 and 130 ^{o} C, respectively, with the HTF inlet temperature of 40 ^{o} C.

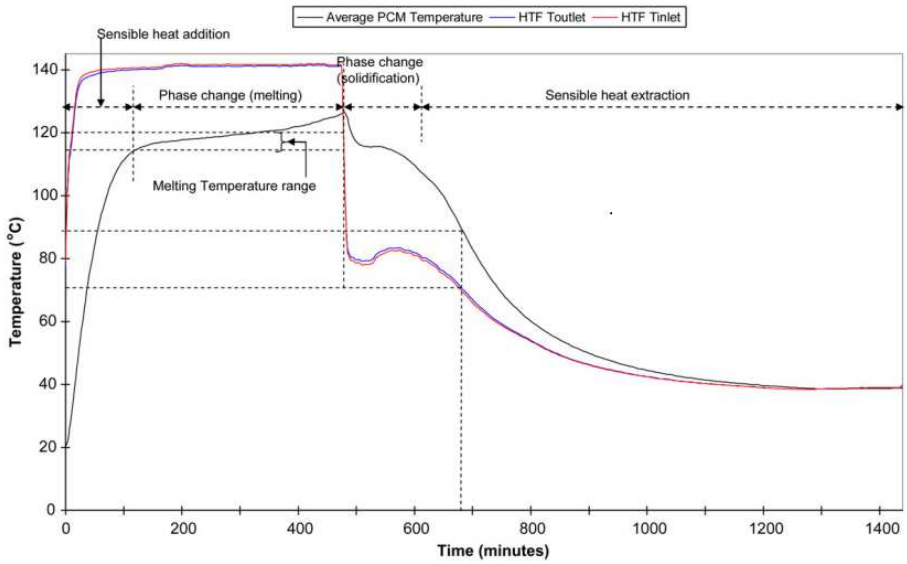

Figure 3.3 Average temperature measured in the longitudinal finned PCM system during charging and discharging (Agyenim et al., 2010)

In order to use an optimum grid size that guaranteed the accuracy requirement and the computing cost, five time steps were tested for the same problem, which is shown in Figure 3.4 (a). For the optimum time step dt =33 s five grid sizes were tested and the number of nodes 250 (axial)* 11(radial) in which dz = 0.004 m and dr = 0.0042 m was chosen for this study, Figure 3.4 (b).

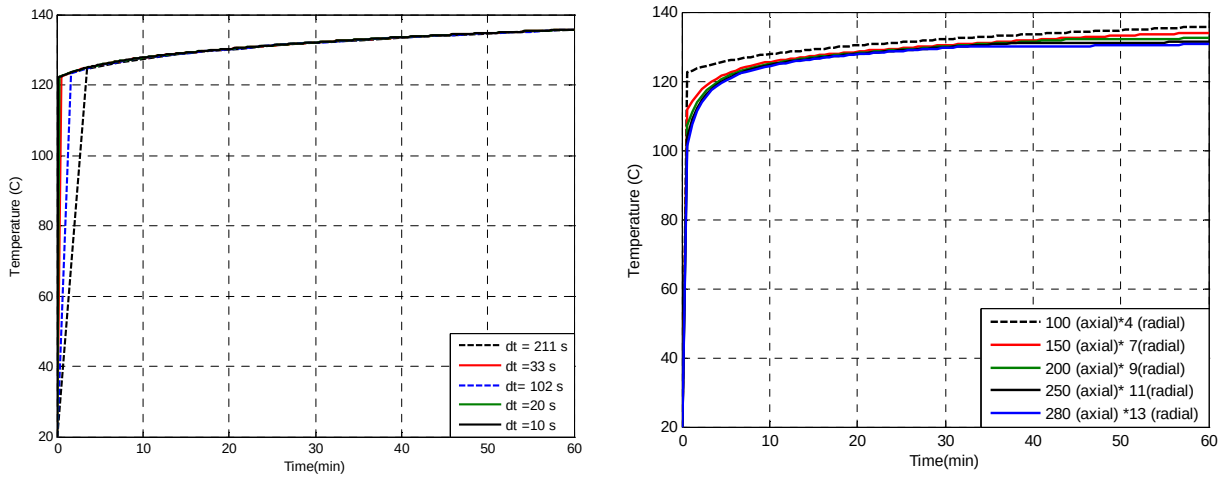

(a) **(b)**

Figure 3.4 Variation of PCM temperature with time for different time step (a) for different number of nodes in axial and radial direction (b)

As it was shown in Figure 3.3 in the experiments the total melting time is about 380 min, which is in good agreement with the numerical results. In the experimental results the longitudinal fins around the outside of the HTF pipe were considered for enhancing the heat transfer of the PCM. In the simulation, the HTF pipe is considered without fins which increases the melting time. On the other hand the convection heat transfer within the PCM and the thickness of the tube are not considered in the simulation while in the reality both play a role. In Figure 3.5, two different locations were considered. The first point is located at x=0 and r = 0.027 m and the second point is at x= 1 and r = 0.073 m.

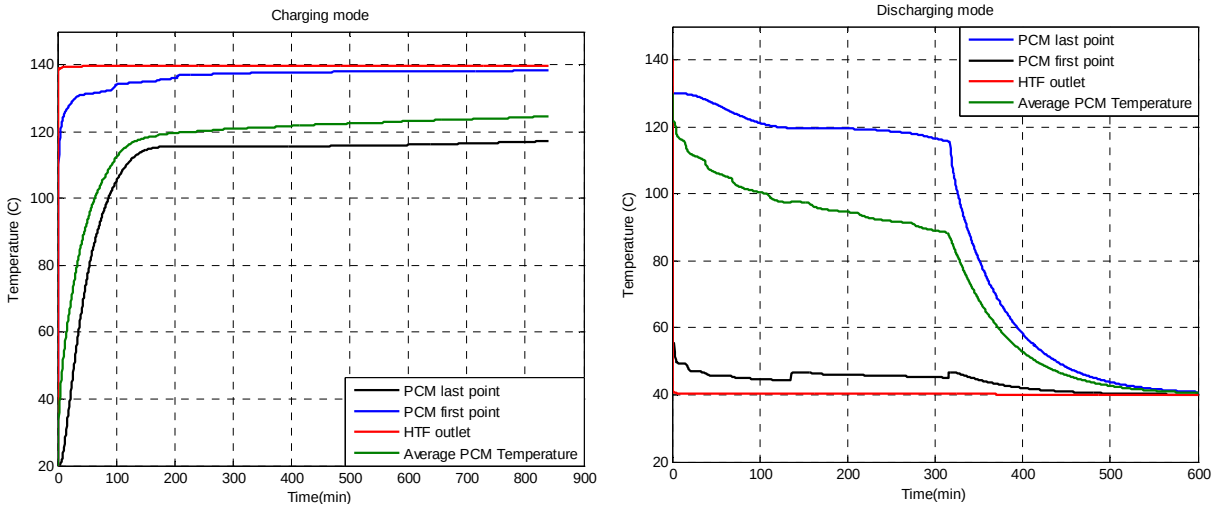

Figure 3.5 The simulated results for the charging and discharging mode

The variation of PCM melting time with pipe diameter for two HTF inlet temperatures is shown in Figure 3.6. By increasing the tube diameter the PCM melting time decreases, due to the increase of the heat transfer area. The PCM melting time increases as the HTF inlet temperature decreases.

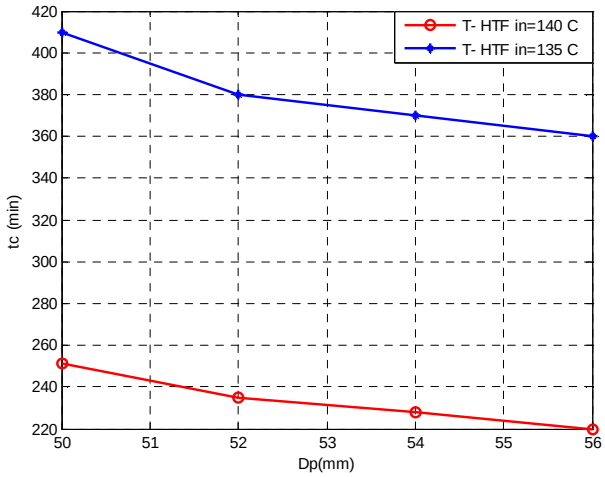

Figure 3.6 Variation of pipe diameter with melting time for two inlet HTF temperature

In Figure 3.7 the variation of PCM melting time with HTF mass flow rate is shown at constant HTF inlet temperature. As it was expected, increasing the mass flow rate decreases the PCM melting time due to the increased velocity of the HTF and the related improved convection heat transfer coefficient.

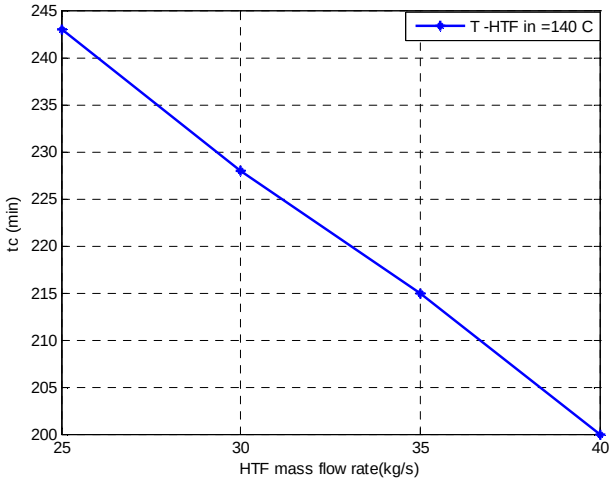

Figure 3.7 Variation of HTF mass flow rate with PCM melting time

3.5 Conclusions

The mathematical model for the latent heat storage unit was developed in this chapter. Applying the finite difference method and the enthalpy approach, the coupled governing partial differential equations of the PCM container and the heat transfer fluid were numerically solved. The model was implemented in MATLAB. For the validation Erythritol is considered as a PCM and a good agreement between the experimental results and numerical results were obtained. The behavior of the system with varying three key parameters: HTF inlet temperature, pipe diameter and the HTF mass flow rate were studied. It was observed as the pipe diameter increases the heat transfer area increases which decreases the melting time. The PCM melting time has decreasing trend with increasing the HTF mass flow rate, due to the increase in HTF velocity.

Chapter 4

System Design and Sensitivity Analysis

4.1 Introduction

In Chapters 2 and 3, mathematical models for single effect absorption systems and for latent tube- shell container heat storage were developed and the models were validated with experimental results reported in the literature. In this chapter a specific absorption system and latent heat storage are designed based on the cooling demand of the building mentioned in section 1.4. The systems response is evaluated as a function of several design parameters. Based on the obtained maximum heat transfer rate of generator and the various solar collector area the behavior of the latent heat storage is studied during the discharging and charging times, respectively.

4.2 Absorption system

Based on the cooling requirement (72 kW) of the building mentioned in section 1.4 and the inlet temperature of the external streams the absorption system is designed. The designed input and parameter values for the absorption system are given in Tables 4.1 and 4.2. As it was explained in Chapter 1 the cooling water for the absorber and the condenser is considered to be provided from the Aquifer Thermal Energy Storage (ATES). Therefore, the cooling water temperature which comes from an ATES to the absorption system has the temperature range 12- 15 ^{o}C.

Table 4.1 Designed input conditions for absorption system

Inputs	description	Unit	value
f_g	Hot water mass flow rate	kg/s	4.02
$T_{g,in}$	Hot water inlet temperature	^{o}C	85
f_c	Cooling water mass flow rate	kg/s	6.32
$T_{c,in}$	Cooling water inlet temperature	^{o}C	15
f_e	Chilled water mass flow rate	kg/s	5.54
$T_{e,in}$	Chilled water inlet temperature	^{o}C	12
f_3	Solution mass flow rate	kg/s	0.48

Table 4.2 Designed parameters for the absorption system

Parameters	description	Unit	value
UA_g	Conductance of generator coils	kW/K	5.06
UA_a	Conductance of absorber coils	kW/K	4.75
UA_c	Conductance of condenser coils	kW/K	4.54
UA_e	Conductance of evaporator coils	kW/K	9.06
η_p	Pump efficiency	%	60
ε	Heat transfer effectiveness		0.7

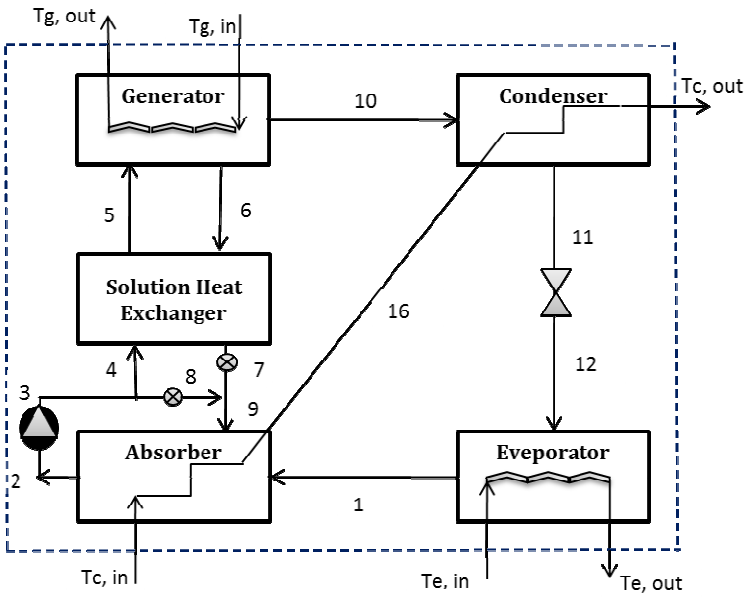

Figure 4.1 The absorption cooling cycle

4.3 Results and discussions

The performance of the designed system is obtained with the developed SIMULINK model and is given in Tables 4.3 and 4.4. The corresponding cycle is shown in Figure 4.2.

Table 4.3 Calculated parameters for the designed absorption system

State point	Description	Temperature ^{o}C	Mass flow rate Kg/s	Concentration %
1	Vapor from evaporator to absorber	2.40	0.03	-
2	Weak solution outlet from absorber	31.5	0.48	55
3	Weak solution outlet from solution pump	31.5	0.48	55
4	Weak solution inlet to heat exchanger	31.5	0.24	55
5	Weak solution inlet to generator	54.64	0.24	55
6	Strong solution outlet from generator	73.30	0.22	62.73
7	Strong solution outlet from heat exchanger	44	0.22	62.73
8	Weak solution outlet from solution pump	31.5	0.24	55
9	Intermediate solution inlet to absorber	38.33	0.46	58.61
10	Superheated vapor from generator to condenser	56.64	0.03	-
11	Condensate from condenser to expansion valve	24.61	0.03	-
16	Outlet cooling water from absorber	18.27	6.32	
	Outlet cooling water from condenser	21	6.32	
	Chilled water outlet from evaporator	8.89	5.54	-
	Hot water outlet from generator	79.8	4.02	

Table 4.4 Calculated parameters for the designed absorption system

	Description	Unit	Value
Q_e	Evaporator heat transfer rate	kW	72.05
Q_c	Condenser heat transfer rate	kW	74.23
Q_g	Generator heat transfer rate	kW	88.82
Q_a	Absorber heat transfer rate	kW	86.64
COP	Coefficient of performance		0.81

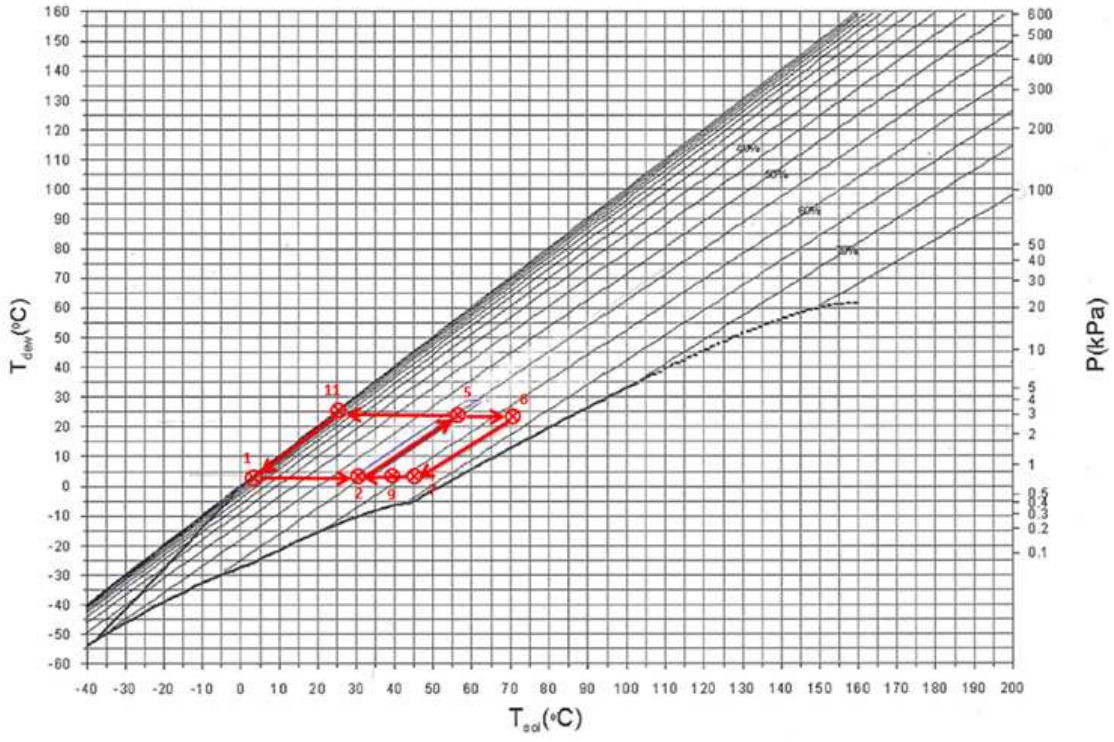

Figure 4.2 Temperature- pressure diagram of absorption cooling cycle

As it is shown in Figure 4.2, regarding to the condensing and evaporating temperature, 2.4 and 24.61 ^{o}C, respectively, the inlet hot water temperature should be between 55 and 85 ^{o}C to prevent LiBr crystallization. The model with the designed conditions is validated qualitatively. As it is shown in Figure 4.3 (a), by increasing the hot water temperature the COP decreases. The same trend was obtained experimentally by Asdrubali and Grignaffini (2005). Increasing the hot water temperature, increases the heat exchanged at the generator more than the heat exchanged at the evaporator, so that the COP decreases.

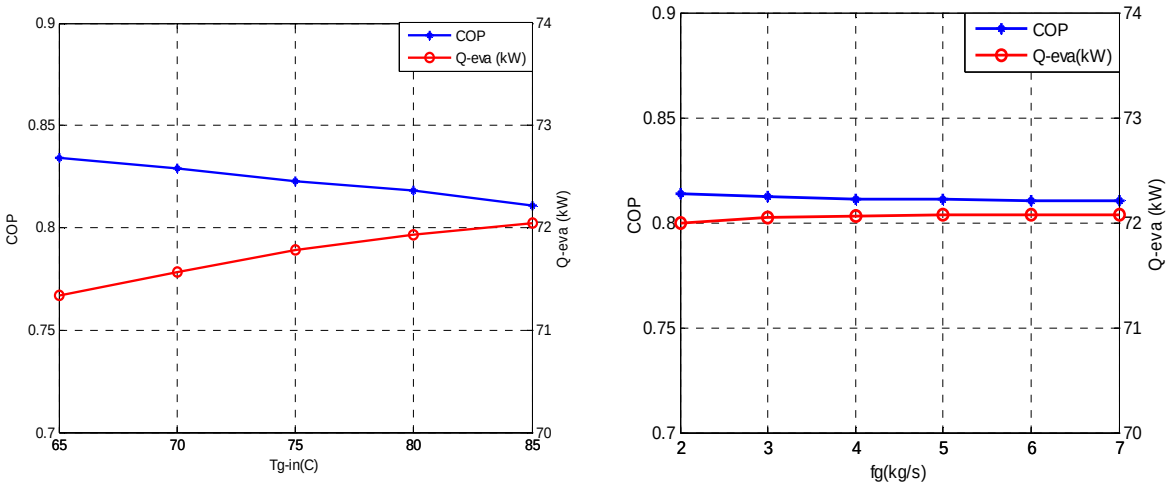

(a) **(b)**

Figure 4.3 Variation of COP and cooling capacity with hot water temperature(a) and mass flow rate (b)

As it is shown in Figure 4.3 (b) variation of the mass flow rate does not change the COP and the evaporator heat transfer rate significantly. Bakhtiari et al. obtained a similar trend as obtained from the simulation results (Bakhtiari *et al.*, 2010) .

The variation of COP and cooling capacity with chilled water inlet temperature and mass flow rate is shown in Figure 4.4. Increasing the chilled inlet water temperature increases the COP and evaporator heat transfer rate. Variation of COP and the cooling capacity in not considerable with increasing chilled water mass flow rate.

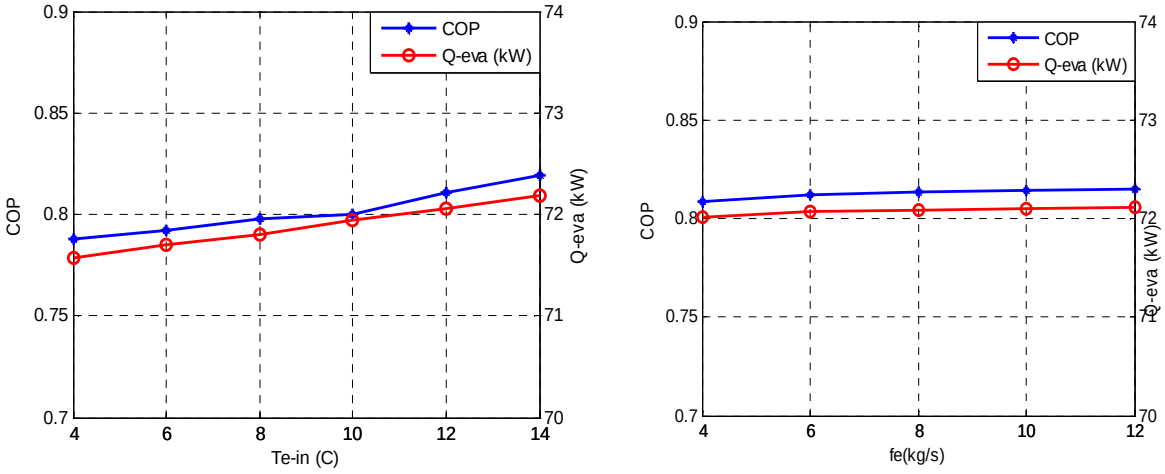

(a) **(b)**

Figure 4.4 COP and the cooling capacity vs. chilled water temperature (a) and mass flow rate (b)

The variation of inlet cooling water temperature and mass flow rate with COP and cooling capacity is shown in Figure 4.5. Same as the results obtained by Bakhtiari et al. (2010), increasing the inlet cooling water temperature and mass flow rate has significant effect on the COP. The cooling capacity increases as the cooling water mass flow rate increases and has a decreasing trend as the inlet cooling water temperature increases.

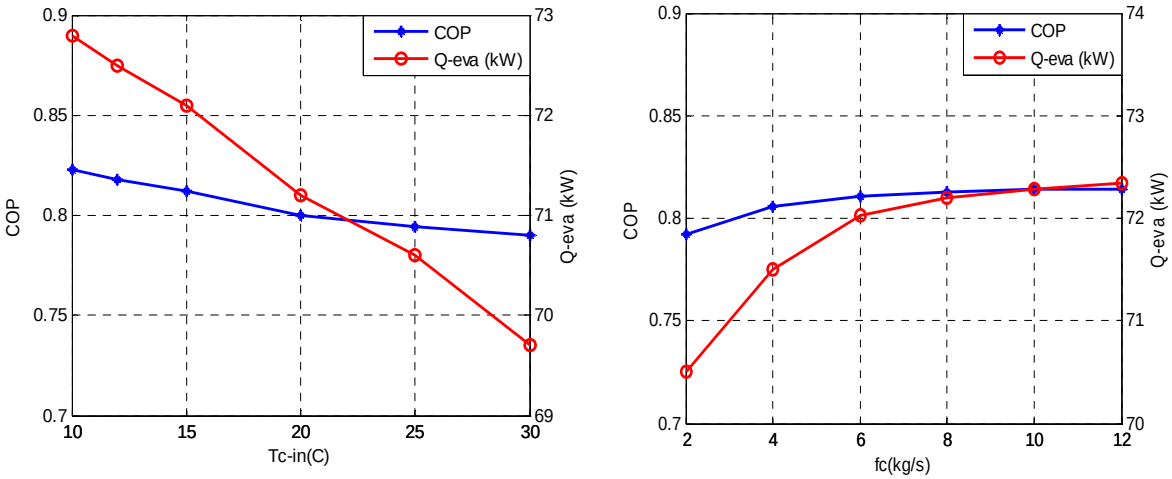

(a) **(b)**

Figure 4.5 COP and cooling capacity vs. cooling water temperature (a) and mass flow rate(b)

4.4 Latent heat storage

In designing the latent heat storage unit, selection of the PCM is an important factor which depends on the application. In the previous section, the absorption system was designed based on the cooling demand of the building. For the designed absorption system hot water temperature in the range of 55 – 85 ^{o} C should be provided. Unfortunately, the thermo-physical properties of PCM's in the melting temperature range of 80 -140 ^{o}C have not been studied sufficiently. Therefore, from the PCM 's which were given in Tables 1.7 and 1.6, in Chapter 1, Erythitol is selected as a latent heat storage material for which the thermo-physical properties are available in the literatures. Erythritol has a high heat of fusion and since the melting temperature is high the discharge time will be longer among the other PCM's to apply for the absorption system.

For designing the latent heat storage unit the mass of PCM, number of tubes, radius of the tubes and the HTF mass flow rate should be obtained which are important parameters on the storage efficiency and the PCM melting and solidification time. The geometry parameters of the designed latent heat storage are given in Table 4.5. The mass flow rate of HTF (water) is obtained in section 4.2, for the designed absorption system. For designing the latent heat storage, it is considered that the storage consists of 20 unit.

Table 4.5 The geometry parameters of designed PCM storage for one unit

Property	Value	Unit
Mass of PCM	500	kg
HTF mass flow rate	0.2	kg/s
Number of tubes	70	-
Length of the tubes	1.40	m
Radius of tubes	0.0055	m
Radius of PCM cylinder (one module)	0.0357	m

For the charging process it is considered that the PCM is in the solid state with the temperature of 20 ^{o}C and the HTF with temperature of 135 ^{o}C flows through the tubes. The variation of the PCM temperature for one module in two locations, average PCM temperature and the HTF outlet temperature are shown in Figure 4.6. The PCM first point is located at r = 0.0055 m and x= 0 m and the second point is located at r = 0.0357 m and x=1.4 m.

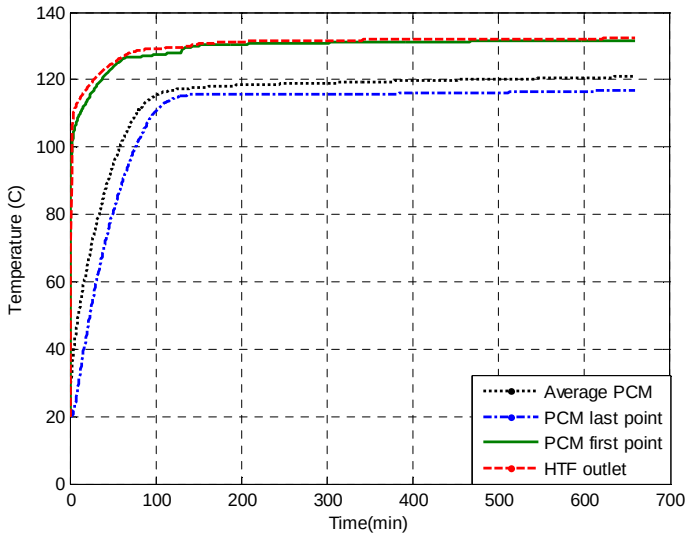

Figure 4.6 Variation of HTF outlet temperature and PCM temperature in two locations of the cylinder and the average PCM temperature with time in charging mode

The storage efficiency is defined as the ratio of the energy stored to the maximum energy that could be stored in the latent heat storage. In Figure 4.7 the variation of storage efficiency with time is shown. The storage has its maximum energy when the whole PCM is melted and reaches the HTF inlet temperature.

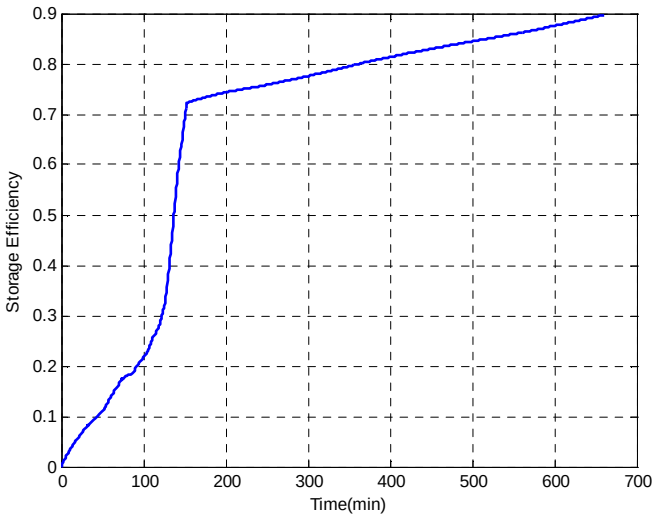

Figure 4.7 Variation of storage efficiency with time for charging mode

The behavior of the designed PCM storage during the discharging process is also studied. In this case the initial temperature of the whole PCM and HTF inlet temperature are considered as 130 ^{o}C and 85 ^{o}C, respectively. As it is shown in Figure 4.8 it takes more than 11 hours that the PCM temperature reaches the HTF inlet temperature.

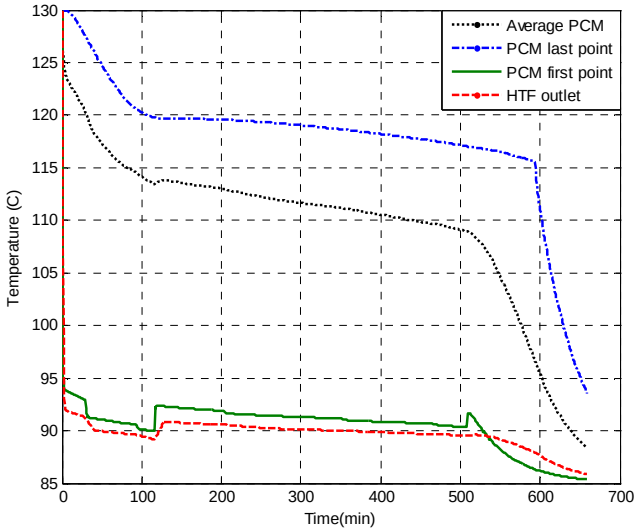

Figure 4.8 Variation of HTF outlet temperature and PCM temperature in two locations of the cylinder and the average PCM temperature with time in discharging mode

4.5 Sensitivity analysis of the designed latent heat storage

The geometry of the PCM storage, mass of PCM and HTF mass flow rate effect the storage efficiency and the PCM melting time. In Figure 4.9 the variation of storage efficiency and the PCM melting time with number of tubes is shown. The length of tubes, mass of PCM and the HTF mass flow rates are held constant. The storage efficiency is obtained for all cases at t= 300 min. Varying the number of tubes changes the tube radius and the radius of PCM cylinder. As it is observed in the figure the storage efficiency has increasing trend with the increasing number of pipes, and the PCM melting time has decreasing trend with increasing the number of tubes. This behavior of the PCM is due to the increasing of convective heat transfer coefficient due to the increasing of HTF Reynolds number with increasing the number of pipes inside the storage unit.

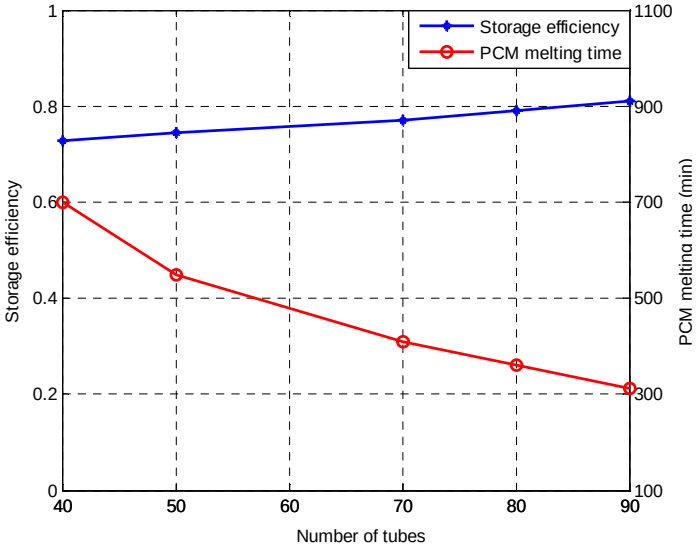

Figure 4.9 Variation of storage efficiency and PCM melting time with number of tubes

The variation of the storage efficiency and the PCM melting time as a function of mass of PCM is shown in Figure 4.10. In this case the number of tubes and the tube radius, the length of tubes and the HTF mass flow rate are held constant as given in Table 4.5. Varying the PCM ‘s mass effects the radius of PCM cylinder. Increasing the mass of PCM with the fixed tube radius increases the radius of PCM cylinder. Therefore the thickness between the tube radius and the radius of PCM cylinder increases. As it is shown in Figure 4.10, the storage efficiency and the PCM melting time have decreasing and increasing trends, respectively, as the PCM ‘s mass increases.

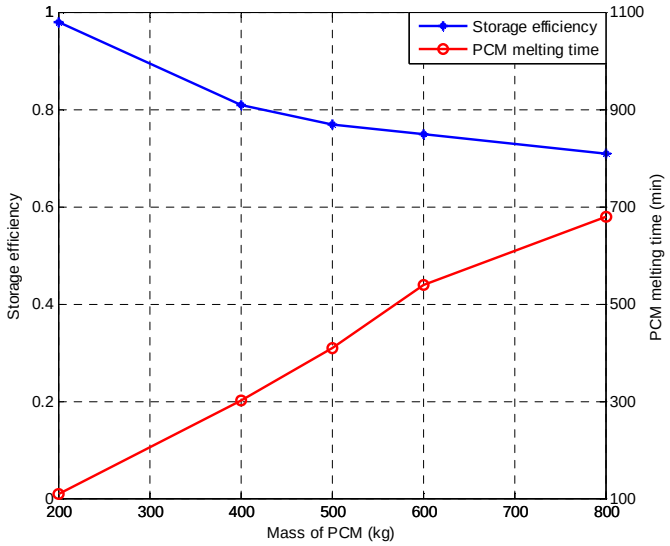

Figure 4.10 Variation of storage efficiency and PCM melting time with mass of PCM

In Figure 4.11, the variation of storage efficiency and the PCM melting time with the tube radius is shown. In this case the mass of PCM, number of tubes, length of tubes and the HTF mass flow rate are held constant. As it was expected, as the tube radius increases the HTF velocity decreases. Therefore the time that HTF flows through the tubes increases which increases the storage efficiency and decreases the PCM melting time.

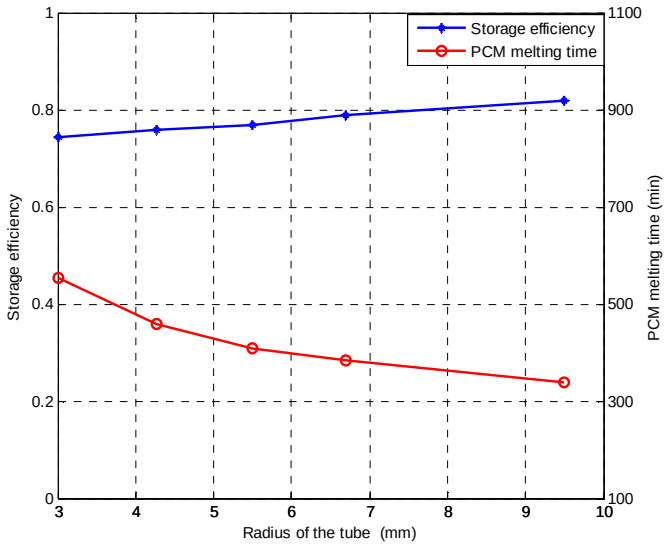

Figure 4.11 Variation of storage efficiency and PCM melting time with tube radius

4.6 Latent heat storage integrated with solar collector

For charging the designed latent heat storage the inlet temperature of the HTF flow into the storage should be higher than the PCM melting temperature. Evacuated tube solar collectors can provide temperatures higher than 120 ^{o} C. In Figure 4.12 the variation of solar radiation and ambient temperature which is coupled to the latent heat storage for a specific day of July in the Netherlands from 6:00 a.m. to 22 p.m. is shown.

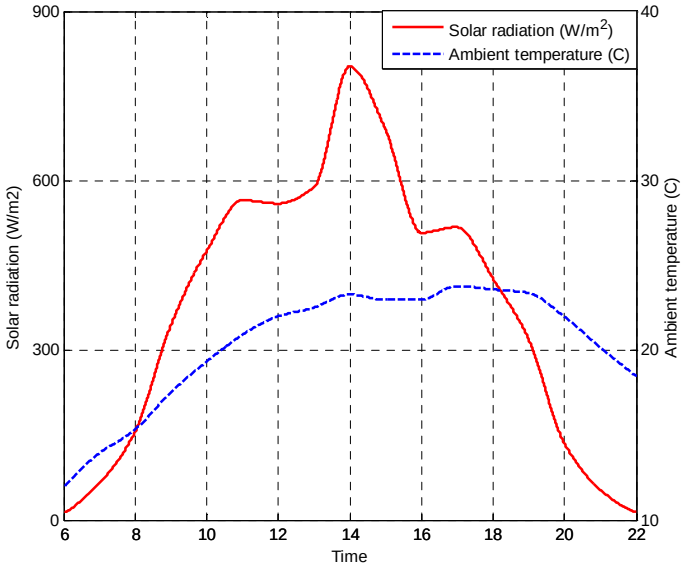

Figure 4.12 Variation of solar radiation and ambient temperature for a specific July day in the Netherlands

The variation of PCM temperature with time for various solar collector areas for one unit of latent heat storage is shown in Figure 4.13. It is observed that, as the solar collector area increases, the PCM reaches its melting time earlier. The PCM storage starts to discharge as the solar radiation decreases and the heat transfer rate from the HTF to the PCM decreases.

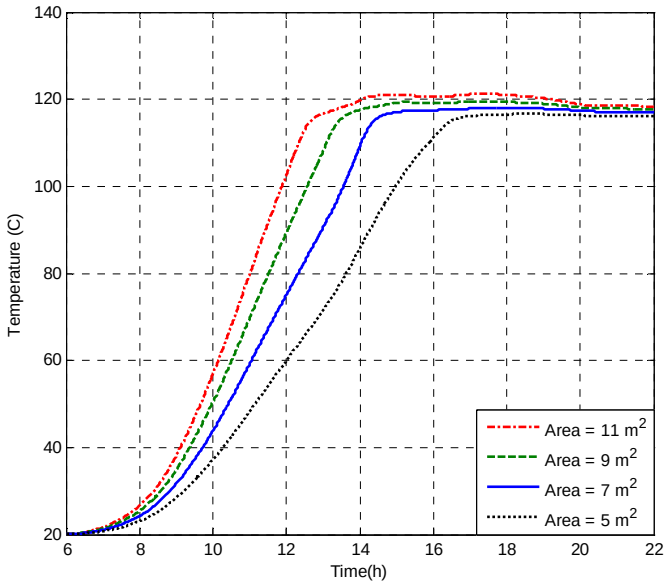

Figure 4.13 Variation of PCM temperature with time for various evacuated tube solar collector areas

4.7 Absorption system integrated with latent heat storage

The discharging behavior of the designed latent heat storage with the maximum heating requirement of the generator (89 kW) is shown in Figure 4.14. In this case the initial temperature of the PCM and the HTF are considered 130 and 20 ^{o}C, respectively. As it was mentioned before the HTF outlet temperature of the storage should be in the range of 55 – 85 ^{o} C. As it is shown in the figure the storage system could provide for 10 hours the requested HTF outlet temperature for driving the generator.

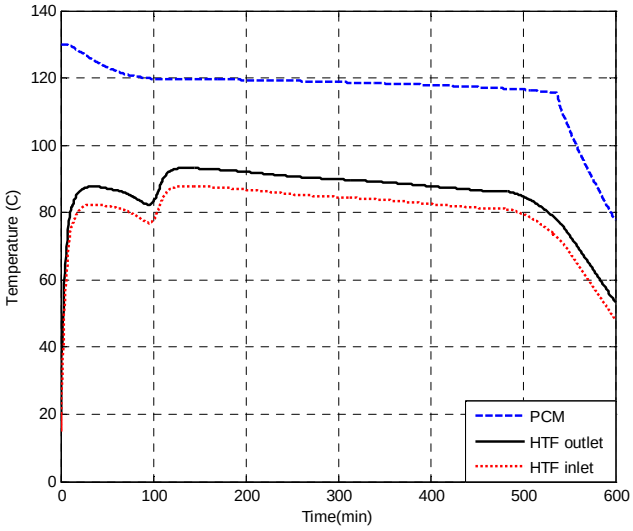

Figure 4.14 Variation of PCM solidification with time for the maximum heating requirment of the generator

The peaks which could be observed in the figure are due to the large difference between the thermal conductivity of PCM in the solid and liquid phases.
The discharging process of the latent heat storage unit is studied for the maximum heating demand of the generator due to maximum demand of the cooling load. The building has its maximum cooling load for less than 6 hours. Therefore, for the lower cooling load the heating demand of the generator will be decreased which decreases the difference between the hot water inlet and outlet temperature. Therefore, in general, the discharging duration will be more than what is obtained for maximum demand of the generator.

4.8 Economic Analysis

The whole system consists of a single effect absorption cooling cycle, an evacuated tube solar collector field, the PCM storage and the PCMs. For providing the cooling water to the absorption system it is considered that an aquifer thermal energy storage is already available in the Schiphol airport. So, its costs are not considered. In Table 4.6 the specific price of each major component in the system is given. For evaluating the cost of PCM storage the Hall equations (1990) for evaluating the installed cost of shell and tube heat exchanger for stainless steel shell and tube heat exchanger is used.

Table 4.6 The specific price of major components

	Reference	Price	Unit
	Henning (2007)	400	€/ kW $_{cool}$
Single effect absorption system	Kim & Infante Ferreira (2008)	400	€/ kW $_{cool}$
	Mokhtar et al. (2010)	250	€/ kW $_{cool}$
Evacuated tube solar collector	Gebreslassie et al. (2010)	771	€/m^2
PCM (Erythritol)	Kakiuchi et al. (1998)	3.5	€/kg
PCM storage	Hall et al. (1990)	0.69 (10,000 + 324 $A^{0.91}$)	€

The size of each major component, its price and the total price of the system are given in Table 4.7. The percentages of the total cost of the different system components is shown in Figure 4.15. The evacuated tube solar collector field encompass approximately 71 % of the total cost. The next category is the PCM (Erythritol) itself.

Table 4.7 The size and price of major components of the system

Component	Size	unit	Price (€)
Single effect absorption	72	kW	18,000
Evacuated tube solar collector	220	m^2	169,620
PCM (Erythritol)	10,000	kg	35,000
PCM buffer	68	m^2	17,300
Total			239,920

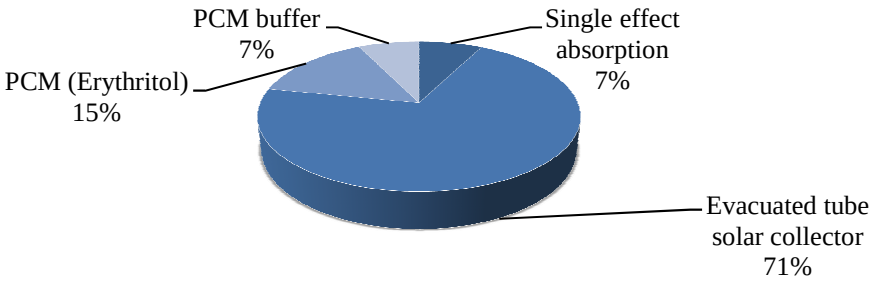

Figure 4.15 Pie chart of the total system costs

The cost of the system could be decreased by replacing the PCM (Erythritol) with a PCM which has a melting temperature lower than Erythritol. Therefore, the required solar collector area will be significantly decreased which has significant effect on the system capital cost. The evacuated tube solar collector field could be replaced by flat plate solar collector field if a PCM which has melting temperature lower than 100 ^oC is used. The price of flat plat solar collector is one third of evacuated solar collector (Gebreslassie *et al.*, 2010). Since the thermo- physical properties of the PCM's which have the melting temperatures in the range of 90- 100 ^oC have not been studied sufficiently, it is not possible to investigate the behavior of such PCM.

4.9 Conclusions

Regarding to the cooling load of the building (72 kW), the single effect absorption cooling system was designed. The response of the system to the variation of the mass flow rate and temperature of the cooling water, chilled water and hot water were studied. The results showed that increasing the chilled water and hot water mass flow rates does not have significant effect on the performance of the system. On the other hand as the cooling water mass flow rate increases the COP of the system increases. The performance of the system decreases as the hot water and the cooling water temperature increases. And the COP goes up with increasing the chilled water temperature.

Based on the maximum heating demand of the generator, the latent heat storage was designed. Erythritol was considered as the latent heat storage media which has high heat of fusion and the thermo physical properties are available. The transient behavior of the storage during charging and discharging process of the system were investigated. The thermal performance and the melting time of the system with varying the tube radius, mass of PCM and the number of tubes were studied. Increasing the number of tubes and the tube radius increases the storage efficiency and decreases the melting time which is inverse with increasing the mass of PCM.

The discharging process of the latent heat storage integrated with maximum heating demand of generator were studied. The results showed that the system could provide for more than 10 hours the required hot water temperature for driving the air conditioning system.

Chapter 5

Conclusions and Recommendations

5.1 Conclusions

In this study the feasibility of a solar assisted latent heat storage to power a single effect LiBr/ water absorption cooling system was investigated. The thermal behavior of the system has been studied theoretically for a specified building in the Netherlands. A mathematical model for single effect absorption system was developed based on mass balances, energy balances and heat transfer equations and the numerical results were validated by with the data reported from the literature. The absorption system was designed for the maximum cooling load of the specified building (72 kW). The response of the system has been investigated by varying relevant parameters of the system. It was observed that increasing the chilled water and cooling water temperature significantly increases the COP. Varying the hot water and chilled water mass flow rates does not have a considerable effect on the COP and the evaporator heat transfer rate. The COP and the evaporator heat transfer rate improves as the cooling water mass flow rate increases.

For the latent heat storage, the coupled governing partial differential equations of the cylindrical PCM container and the heat transfer fluid were numerically solved using the Finite Difference Method and the enthalpy approach. A good agreement between the obtained results and experimental data reported in the literature was observed. The system response to various parameters e.g. number of tubes, mass of PCM and the HTF mass flow rate was studied. The numerical analysis reveals that, increasing the number of tubes while the PCM's mass, the length of the tube, and the velocity of the HTF are kept constant, improves the storage efficiency and reduces the melting time.

The storage efficiency and the melting time decreases and increases, respectively, as the PCM's mass goes up for constant length, radius and number of tubes. Increasing the mass of PCM leads to thicker layers of PCM surrounding the tubes. The behavior of the system to variation of the HTF velocity was also studied. It was observed that the HTF velocity has an inverse relation with the residence time of the HTF inside the tube. Therefore, the storage efficiency improves and the melting time reduces.

For various evacuated tube solar collector areas, the charging process of the storage for a day in July in the Netherlands was studied. As it was expected, by increasing the collector area, the PCM melts earlier.

The discharging process of the designed latent heat storage for the maximum load of the absorption system was investigated. The results showed that the storage could provide the energy required for driving the cooling system for approximately 10 working hours. The building has its maximum cooling load for less than 6 hours during the hot seasons. Therefore, the designed system could provide the required hot water temperature to drive the generator for more than 10 hours.

The cost of the designed system was also evaluated showing that the evacuated tube solar collector field encompasses 70 % of total cost. This expense can be reduced by decreasing the area of solar collectors, utilizing PCMs with lower melting temperature, and replacing the evacuated tube solar collector with high efficient flat plate solar collectors.

From the environmental point of view, the solar powered single effect absorption system offers a good opportunity to reduce the electricity consumption, hence reduce the consequence CO_2 emission.

5.2 Recommendations for future

- Investigation of the thermo- physical properties of PCMs
- Optimization of the absorption cooling system
- Optimization of the latent heat storage system
- Investigation the behavior of various PCMs integrated with solar assisted absorption cooling system
- Study of the behavior of latent heat storage with different configuration e.g. rectangular and cylindrical (PCM located in the tubes)
- Improvement of the developed computer codes
- Life cycle analysis of the system
- Investigation the behavior of the latent heat storage with the fins on the shell side to increase thermal conductivity in the liquid state
- Study and comparison of the behavior of other solar assisted air conditioning systems integrated with latent heat storage
- Experimental investigation of the system and comparison of the experimental results with numerical studies

References

Abhat, A., 1983. Low temperature latent heat thermal energy storage: heat storage materials. Solar Energy 30, 313-332.

Agyenim, F., Eames, P., Smyth, M., 2010. Experimental study on the melting and solidification behaviour of a medium temperature phase change storage material (Erythritol) system augmented with fins to power a LiBr/H2O absorption cooling system. Renewable Energy.

Agyenim, F., Rhodes, M., Knight, I., 2007. The use of phase change material (PCM) to improve the coefficient of perform-ance of a chiller for meeting domestic cooling in Wales. 2nd PALENC Conference and 28th AIVC Conference on Building Low Energy Cooling and Advanced Ventilation Technologies in the 21sr Century, Crete island, Greece.

Asdrubali, F., Grignaffini, S., 2005. Experimental evaluation of the performances of a H2O-LiBr absorption refrigerator under different service conditions. International Journal of Refrigeration 28, 489-497.

ASHRAE, 2009. ASHRAE handbook: fundamentals. American Society of Heating, Refrigerating, and Air-Conditioning Engineers.

Bakhtiari, B., Fradette, L., Legros, R., Paris, J., 2010. A model for analysis and design of H2O-LiBr absorption heat pumps. Energy Conversion and Management.

Balaras, C.A., Grossman, G., Henning, H.M., Infante Ferreira, C.A., Podesser, E., Wang, L., Wiemken, E., 2007. Solar air conditioning in Europe--an overview. Renewable and Sustainable Energy Reviews 11, 299-314.

Bonacina, C., Comini, G., Fasano, A., Primicerio, M., 1973. Numerical solution of phase-change problems. International journal of heat and mass transfer 16, 1825-1832.

Carslaw, H.S., Jaeger, J.C., 1959. Conduction of heat in solids. Oxford: Clarendon Press, 1959, 2nd ed. 1.

Cascales, J., García, F.V., Izquierdo, J., Marín, J., Sánchez, R.M., 2010. Modelling an absorption system assisted by solar energy. Applied Thermal Engineering.

CBS, 2007. Dutch gas and electricity prices among the highest in Europe.

Comini, G., Del Guidice, S., Lewis, R., Zienkiewicz, O., 1974. Finite element solution of non linear heat conduction problems with special reference to phase change. International Journal for Numerical Methods in Engineering 8, 613-624.

Costa, M., Buddhi, D., Oliva, A., 1998. Numerical simulation of a latent heat thermal energy storage system with enhanced heat conduction. Energy Conversion and Management 39, 319-330.

Costa, M., Oliva, A., Segarra, C., Alba, R., 1991. Numerical simulation of solid-liquid phase change phenomena. Computer methods in applied mechanics and engineering 91, 1123-1134.

Dinçer, I., Rosen, M., 2011. Thermal energy storage: systems and applications. Wiley.

Elsafty, A., Al-Daini, A., 2002. Economical comparison between a solar-powered vapour absorption air-conditioning system and a vapour compression system in the Middle East. Renewable energy 25, 569-583.

Esen, M., 2000. Thermal performance of a solar-aided latent heat store used for space heating by heat pump. Solar Energy 69, 15-25.

Esen, M., Ayhan, T., 1996. Development of a model compatible with solar assisted cylindrical energy storage tank and variation of stored energy with time for different phase change materials. Energy Conversion and Management 37, 1775-1785.

Farid, M.M., Khudhair, A.M., Razack, S.A.K., Al-Hallaj, S., 2004. A review on phase change energy storage: materials and applications. Energy Conversion and Management 45, 1597-1615.

Florides, G.A., Kalogirou, S.A., Tassou, S., Wrobel, L., 2003. Design and construction of a LiBr-water absorption machine. Energy Conversion and Management 44, 2483-2508.

Fong, K., Chow, T., Lee, C., Lin, Z., Chan, L., 2010. Comparative study of different solar cooling systems for buildings in subtropical city. Solar Energy 84, 227-244.

Gebreslassie, B.H., Guillén-Gosálbez, G., Jiménez, L., Boera, D., 2010. A systematic tool for the minimization of the life cycle impact of solar assisted absorption cooling systems. Energy.

Gomri, R., 2010. Investigation of the potential of application of single effect and multiple effect absorption cooling systems. Energy Conversion and Management 51, 1629-1636.

Gordon, J.M., Choon Ng, K., 2000. High-efficiency solar cooling. Solar Energy 68, 23-31.

Hall, S., Ahmad, S., Smith, R., 1990. Capital cost targets for heat exchanger networks comprising mixed materials of construction, pressure ratings and exchanger types. Computers & chemical engineering 14, 319-335.

Helm, M., Keil, C., Hiebler, S., Mehling, H., Schweigler, C., 2009. Solar heating and cooling system with absorption chiller and low temperature latent heat storage: Energetic performance and operational experience. International Journal of Refrigeration 32, 596-606.

Henning, H., 2007. Solar assisted air conditioning of buildings-an overview. Applied Thermal Engineering 27, 1734-1749.

Herold, K.E., Radermacher, R., Klein, S.A., 1996. Absorption chillers and heat pumps. CRC.

Jeong, S., Garimella, S., 2002. Falling-film and droplet mode heat and mass transfer in a horizontal tube LiBr/water absorber. International journal of heat and mass transfer 45, 1445-1458.

Jones, B.J., Sun, D., Krishnan, S., Garimella, S.V., 2006. Experimental and numerical study of melting in a cylinder. International Journal of Heat and Mass Transfer 49, 2724-2738.

Joudi, K.A., Lafta, A.H., 2001. Simulation of a simple absorption refrigeration system. Energy Conversion and Management 42, 1575-1605.

Kakiuchi, H., Yamazaki, M., Yabe, M., Chihara, S., Terunuma, Y., Sakata, Y., Usami, T., 1998. A study of erythritol as phase change material. IEA Annex, 11-13.

Kalogirou, S.A., 2004. Solar thermal collectors and applications. Progress in energy and combustion science 30, 231-295.

Kaygusuz, K., 1995a. Experimental and theoretical investigation of latent heat storage for water based solar heating systems. Energy Conversion and Management 36, 315-323.

Kaygusuz, K., 1995b. Performance of solar-assisted heat-pump systems. Applied Energy 51, 93-109.

Kenisarin, M., Mahkamov, K., 2007. Solar energy storage using phase change materials. Renewable and Sustainable Energy Reviews 11, 1913-1965.

Kim, D., Infante Ferreira, C., 2008. Solar refrigeration options-a state-of-the-art review. International journal of Refrigeration 31, 3-15.

Lacroix, M., 1993. Numerical simulation of a shell-and-tube latent heat thermal energy storage unit. Solar Energy 50, 357-367.

Lane, G.A., 1983. Solar heat storage: latent heat materials. CRC Press,Boco Raton, FL.

Lazaridis, A., 1970. A numerical solution of the multidimensional solidification (or melting) problem. International journal of heat and mass transfer 13, 1459-1477.

Lee, R., DiGuilio, R., Jeter, S., Teja, A., 1990. Properties of lithium bromide–water solutions at high temperatures and concentration. II. Density and viscocity. ASHRAE Trans 96, 709-728.

Lee, S.F., Sherif, S., 2001. Thermodynamic analysis of a lithium bromide/water absorption system for cooling and heating applications. International journal of energy research 25, 1019-1031.

Li, Z., Sumathy, K., 2000. Technology development in the solar absorption air-conditioning systems. Renewable and Sustainable Energy Reviews 4, 267-293.

Löf, G., Tybout, R., 1974. The design and cost of optimized systems for residential heating and cooling by solar energy. Solar Energy 16, 9-18.

Lorton, R., Gilchrist, K., Green, R., 2000. Development and operation of a high performance 10kw absorption chiller* 1: Développement et fonctionnement d'un refroidisseur haute performance à absorption d'une capacité de 10 kW. International journal of refrigeration 23, 572-576.

Mayhew, Y.R., Rogers, G.F.C., 1994. Thermodynamic and transport properties of fluids: SI units. Basil Blackwell.

Mokhtar, M., Ali, M.T., Bräuniger, S., Afshari, A., Sgouridis, S., Armstrong, P., Chiesa, M., 2010. Systematic comprehensive techno-economic assessment of solar cooling technologies using location-specific climate data. Applied Energy.

Ng, K., Bong, T., Chua, H., Bao, H., 1994. Theoretical and experimental analysis of an absorption chiller: Analyse théorique et expérimentale d'un groupe refroidisseur absorption. International journal of refrigeration 17, 351-358.

Qi, Q., Deng, S., Jiang, Y., 2008. A simulation study on a solar heat pump heating system with seasonal latent heat storage. Solar Energy 82, 669-675.

Raj, V., Velraj, R., 2010. Review on free cooling of buildings using phase change materials. Renewable and Sustainable Energy Reviews 45, 1597-1615.

Riffat, S., Qiu, G., 2004. Comparative investigation of thermoelectric air-conditioners versus vapour compression and absorption air-conditioners. Applied Thermal Engineering 24, 1979-1993.

Schröder, J., Gawron, K., 1981. Latent heat storage. International Journal of Energy Research 5, 103-109.

Sharma, A., Tyagi, V., Chen, C., Buddhi, D., 2009. Review on thermal energy storage with phase change materials and applications. Renewable and Sustainable Energy Reviews 13, 318-345.

Stritih, U., Butala, V., 2007. Energy saving in building with PCM cold storage. Int. J. Energy Res 31, 1532-1544.

Tan, F., 2008. Constrained and unconstrained melting inside a sphere. International Communications in Heat and Mass Transfer 35, 466-475.

Tyagi, V., Buddhi, D., 2007. PCM thermal storage in buildings: A state of art. Renewable and Sustainable Energy Reviews 11, 1146-1166.

Vynnycky, M., Kimura, S., 2007. An analytical and numerical study of coupled transient natural convection and solidification in a rectangular enclosure. International Journal of Heat and Mass Transfer 50, 5204-5214.

Vyshak, N., Jilani, G., 2007. Numerical analysis of latent heat thermal energy storage system. Energy Conversion and Management 48, 2161-2168.

Wilbur, P.J., Manchini, T.R., 1976. A comparison of solar absorption air conditioning systems. Solar Energy 18, 569-576.

Yoo, J., Rubinsky, B., 1983. Numerical computation using finite elements for the moving interface in heat transfer problems with phase transformation. Numerical Heat Transfer, Part A: Applications 6, 209-222.

Zalba, B., Marin, J., Cabeza, L., Mehling, H., 2003. Review on thermal energy storage with phase change: materials, heat transfer analysis and applications. Applied Thermal Engineering 23, 251-283.

Zhang, S., Niu, J., 2010. Experimental investigation of effects of supercooling on microencapsulated phase-change material (MPCM) slurry thermal storage capacities. Solar Energy Materials and Solar Cells 94, 1038-1048.

Zogou, O., Stamatelos, A., 1998. Effect of climatic conditions on the design optimization of heat pump systems for space heating and cooling. Energy Conversion and Management 39, 609-622.

Appendix A

A.1. LiBr solution and refrigerant pressure and temperatures

Range $45\% < X < 70\%$ LiBr
T_{sol} = solution temperature (°C), range $5 < T_{sol} < 175$ °C
T_{ref} = refrigerant saturated temperature (°C), range $-15 < T_{ref} < 110$ °C
P = saturation pressure (kPa)
$A_0 = -2.00755$, $A_1 = 0.16976$, $A_2 = -0.003133362$, $A_3 = 0.0000197668$
$B_0 = 124.937$, $B_1 = -7.71649$, $B_2 = 0.152286$, $B_3 = -0.0007959$
$\Sigma A = A_0X^0 + A_1X^1 + A_2X^2 + A_3X^3$
$\Sigma B = B_0X^0 + B_1X^1 + B_2X^2 + B_3X^3$
$C = 7.05$, $D = -1596.49$, $E = -104095.5$
$\mathrm{Log}P = C + D/(T_{ref} + 273) + E/(T_{ref} + 273)^2$
$T_{ref} = (-2E/(D + [D^2 - 4E(C - \log P)]^{0.5})) - 273$
$T_{sol} = \Sigma B + T_{ref}\Sigma A$

A.2 Enthalpy of LiBr solution

Range $40\% < X < 70\%$ LiBr
T = solution temperature (°C)
h = enthalpy (kJ/kg)
Solution temperature range 15 °C $< T <$ 165 °C
$A_0 = -2024.33$, $A_1 = 163.309$, $A_2 = -4.88161$, $A_3 = 0.06302948$, $A_4 = -0.0002913704$
$B_0 = 18.2829$, $B_1 = -1.1691757$, $B_2 = 0.03248041$, $B_3 = -0.0004034184$, $B_4 = 0.0000018520569$
$C_0 = -0.037008214$, $C_1 = 0.0028877666$, $C_2 = -0.000081313015$
$C_3 = 0.00000099116628$, $C_4 = -0.0000000044441207$
$\Sigma A = A_0X^0 + A_1X^1 + A_2X^2 + A_3X^3 + A_4X^4$
$\Sigma B = B_0X^0 + B_1X^1 + B_2X^2 + B_3X^3 + B_4X^4$
$\Sigma C = C_0X^0 + C_1X^1 + C_2X^2 + C_3X^3 + C_4X^4$
$h = \Sigma A + T\,\Sigma B + \Sigma C\,T^2$

A.3. Density of LiBr solution

Range $20\% < X < 60\%$
T = solution temperature (°C), $0 < T < 200$ °C,
ρ_x = LiBr solution density (kg/m^3)
$X_0 = X/100$
$\rho_x = 1145.36 + 470.84X_0 + 1374.79X_0^2 - (0.33339 + 0.571749X_0)(273 + T)$

A.4. Specific heat of LiBr solution (curve fit from Ref. —$R^2 = 0.9997$)

X = %LiBr
C_P = specific heat of LiBr solution (J/kg K)
$C_P = 0.0976X^2 - 37.512X + 3825.4$

A.5. Saturated water–vapour enthalpy

hg = vapour enthalpy (kJ/kg)
T = temperature (°C)
$hg = -0.00125397T^2 + 1.88060937T + 2500.559$

A.6. Latent heat of condensation of water vapour

h_{fg} = latent heat of condensation (kJ/kg)
T = saturation temperature (°C)
$h_{fg} = -0.00132635T^2 - 2.29983657T + 2500.43063$

A.7. Enthalpy of superheated steam

H_{sh} = enthalpy of superheated steam (kJ/kg),
T_{ref} = refrigerant (water) saturated temperature [see Section 2] (°C)
T_{actual} = temperature of vapour (°C)
P = pressure of vapour (kPa)
T = degrees of superheat (°C)
$T = T_{actual} - T_{ref}$
$H_{SH1} = 32.508 \ln(P) + 2513.2$
$H_{SH2} = 0.00001P^2 - 0.1193P + 2689$
$H_{sh} = ((H_{SH2} - H_{SH1})/100)T + H_{SH1}$

Appendix B

The MATLAB function for the absorber :

```
% Absorber component
function [output]=absorbent(Cpw,f15,T15,T9,UAa,X9,Te,f9,f3,X6,Qa);
%%Outlet water temperature
T16=(Qa/(f15*Cpw))+T15
%Outlet solution temperature
F=@(x) [(Qa/UAa)-(((T9-T16)-(x(1)-T15))/(log((T9-T16)/(x(1)-T15))))];
x0 = [31+273.2];          % Make a starting guess at the solution
Options = optimset('Display','iter');
D = fsolve(F,x0, Options)  % Call optimizer
T2=real(D)
%% Outlet LiBr concentrations
A0=-2.00755;
A1=0.16976;
A2=-0.00313362;
A3=0.0000197668;
B0=124.937;
B1=-7.71649;
B2=0.152286;
B3=-0.0007959;
F=@(x) [(T2-273.2)-((B0*x(1)^0)+(B1*x(1)^1)+(B2*x(1)^2)+(B3*x(1)^3))-
(((A0*x(1)^0)+(A1*x(1)^1)+(A2*x(1)^2)+(A3*x(1)^3))*(Te-273.2))];
x0 = [55.13];          % Make a starting guess at the solution
Options = optimset('Display','iter');
E= fsolve(F,x0, Options);  % Call optimizer
X2=E
%%Outlet solution mass flow rate
f2=f3;
f5=f3/2;
%%Refrigerant mass flow rate
f1=f2-f9;
%%outputs
output(1)=T16;
output(2)=T2;
output(3)=X2;
output(4)=f2;
output(5)=f1;

end
```

The MATLAB function for the solution heat pump :

```
%%Solution heat pump circuits
function [output]=shpc(T2,X2,f2,Te,Tc,etha_P,f1,Pc);
%%Evaporator Pressure calculations
C=7.05;
D=-1596.49;
E=-104095.5;
A=(C+(D/Te)+(E/(Te^2)));
Pe=10^A
%%solution density
X02=X2/100;
rho2=1145.36+(470.84*X02)+(1374.79*X02^2)-((0.333393+(0.571749*X02))*T2)
%%Pump power
W_P=f2*(Pc-Pe)/(rho2*etha_P)
%%Mass conservation
f3=f2;
f4=f2/2;
f8=f2/2;
f5=f4;
f6=f5-f1;
f7=f6;
f9=f7+f8
%%Absorbate concentration
X3=X2;
X4=X2;
X8=X4;
X5=X4;
X6=(f5*X5)/(f6);
X7=X6;
X9=((f2*X2/2)+(f7*X7))/f9;
%%inlet solution temperature to the absorber
A0=-2.00755;
A1=0.16976;
A2=-0.00313362;
A3=0.0000197668;
B0=124.937;
B1=-7.71649;
B2=0.152286;
B3=-0.0007959;
A=((A0*X9^0)+(A1*X9^1)+(A2*X9^2)+(A3*X9^3));
B=((B0*X9^0)+(B1*X9^1)+(B2*X9^2)+(B3*X9^3));
T9=(B+((Te-273.2)*A))+273.2
%%Outputs
output(1)=f9;
output(2)=X9;
output(3)=T9;
output(4)=f4;
output(5)=X4;
output(6)=f6;
output(7)=X6;
output(8)=W_P;
end
```

The MATLAB function for the solution heat exchanger :

```
%%Solution Heat Exchanger
function [ output ] = SHX( f6,T6,X4,f4,X6,etha_HX,Te,Tc)
%%T4 calculation
A0=-2.00755;
A1=0.16976;
A2=-0.00313362;
A3=0.0000197668;
B0=124.937;
B1=-7.71649;
B2=0.152286;
B3=-0.0007959;
A=(A0*X4^0)+(A1*X4^1)+(A2*X4^2)+(A3*X4^3);
B=(B0*X4^0)+(B1*X4^1)+(B2*X4^2)+(B3*X4^3);
T4=(B+((Te-273.2)*A))+273.2
%%T7 Calculation
T7=T6-(etha_HX*(T6-T4))
%%T5 Calculations
Cp4=((0.0976*X4^2)-(37.512*X4)+3825.4);    %Specific heat of LiBr solution(J/kg.K)
Cp6=((0.0976*X6^2)-(37.512*X6)+3825.4);    %Specific heat of LiBr solution(J/kg.K)
T5=(f6*Cp6*(T6-T7)/((f4*Cp4)))+T4
%%Outputs
output(1)=T5;
output(2)=T7;
end
```

The MATLAB function for the Evaporator :

```
%%Evaporator
function [ output ] = evaporator( f1,f13,T13,h11,Cpw,UAe)
F =@(x) [x(1)-(f1*(((-0.00125397*(x(2)-273.2)^2)+(1.88060937*(x(2)-273.2))+2500.559)-h11));
   x(1)-(f13*Cpw*(T13-x(3)));
   x(1)-(UAe*((T13-x(2))-(x(3)-x(2)))/log((T13-x(2))/(x(3)-x(2))))];
x0 = [211/2.89;3+273.2;282];          % Make a starting guess at the solution
Options = optimset('Display','iter');
G = fsolve(F,x0, Options);  % Call optimizer
Qe=G(1,1)
Te=G(2,1)
T14=G(3,1)
output(1)=Qe;
output(2)=Te;
output(3)=T14;
end
```

The MATLAB function for the Condenser :

```
%Condenser
function [ output] = Condenser( f1,f15,T5,T16,Cpw,UAc )
%Conservation of mass
f16=f15;
%%Calculating Qc, Tc, T17
F =@(x) [x(1)-(f1*(((((0.00001*(10^(C+(D/x(2))+(E/(x(2)^2)))^2)-(0.1193*(10^(C+(D/x(2))+(E/(x(2)^2)))))+
2689-(32.508*(C+(D/x(2))+(E/(x(2)^2))))-2513.2)/100)*(T5-
x(2)))+(32.508*(C+(D/x(2))+(E/(x(2)^2))))+2513.2)-
((-0.00125397*(x(2)-273.2)^2)+(1.88060937*(x(2)-273.2))+2500.559)+((-0.0013265*(x(2)-273.2)^2)-
(2.29983657*(x(2)-273.2))+2500.4063)));
x(1)-(f16*Cpw*(x(3)-T16));
x(1)-(UAc*((T5-x(3))-(x(2)-T16))/log((T5-x(3))/(x(2)-T16)))];
x0 = [221/2.89;25+273.2;294];          % Make a starting guess at the solution
Options = optimset('Display','iter');
G = fsolve(F,x0, Options);  % Call optimizer
Qc=G(1,1)
Tc=G(2,1)
T17=G(3,1)
%%Pressure calculations
C=7.05;
D=-1596.49;
E=-104095.5;
A=(C+(D/Tc)+(E/(Tc^2)));
Pc=10^A
%%h11 calculation(kJ/kg)
hg11=((-0.00125397*(Tc-273.2)^2)+(1.88060937*(Tc-273.2))+2500.559);
hfg11=((-0.0013265*(Tc-273.2)^2)-(2.29983657*(Tc-273.2))+2500.4063);
hf11=hg11-hfg11
%outputs
output(1)=Qc;
output(2)=Tc;
output(3)=T17;
output(4)=Pc;
output(5)=hf11;
 end
```

The MATLAB function for the Generator :

```
%Generator
function [ output] =generator(Tc,X6,T5,T18,f18,UAg,Cpw,X4,Pc,f1,f6,f3)
X5=X4;
f5=f3/2;
 %%T6
 A0=-2.00755;
A1=0.16976;
A2=-0.00313362;
A3=0.0000197668;
B0=124.937;
B1=-7.71649;
B2=0.152286;
B3=-0.0007959;
A=(A0*X6^0)+(A1*X6^1)+(A2*X6^2)+(A3*X6^3);
B=(B0*X6^0)+(B1*X6^1)+(B2*X6^2)+(B3*X6^3);
```

```
%%Constants for LiBr solution Enthalpy
Aoh=-2024.33;
A1h=163.309;
A2h=-4.88161;
A3h=0.06302948;
A4h=-0.0002913704;
Boh=18.2829;
B1h=-1.1691757;
B2h=0.03248041;
B3h=-0.0004034184;
B4h=0.0000018520569;
Coh=-0.037008214;
C1h=0.0028877666;
C2h=-0.000081313015;
C3h=0.00000099116628;
C4h=-0.0000000044441207;
C=7.05;
D=-1596.49;
E=-104095.5;
%%Enthalpy at 5
A5=((Aoh*X5^0)+(A1h*X5^1)+(A2h*X5^2)+(A3h*X5^3)+(A4h*X5^4));
B5=((Boh*X5^0)+(B1h*X5^1)+(B2h*X5^2)+(B3h*X5^3)+(B4h*X5^4));
C5=((Coh*X5^0)+(C1h*X5^1)+(C2h*X5^2)+(C3h*X5^3)+(C4h*X5^4));
h5=A5+((T5-273.2)*B5)+(C5*(T5-273.2)^2)
%%Enthalpy at 6
A6=(Aoh*X6^0)+(A1h*X6^1)+(A2h*X6^2)+(A3h*X6^3)+(A4h*X6^4);
B6=(Boh*X6^0)+(B1h*X6^1)+(B2h*X6^2)+(B3h*X6^3)+(B4h*X6^4);
C6=(Coh*X6^0)+(C1h*X6^1)+(C2h*X6^2)+(C3h*X6^3)+(C4h*X6^4);
%%Enthalpy at 10
HSH2=(0.00001*Pc^2)-(0.1193*Pc)+2689;
HSH1=(32.508*log(Pc))+2513.2;
T=(T5-Tc);
A=(C+(D/Tc)+(E/(Tc^2)));
Pc=(10^(C+(D/Tc)+(E/(Tc^2))));
h10=(((((0.00001*(10^(C+(D/Tc)+(E/(Tc^2))))^2)-(0.1193*(10^(C+(D/Tc)+(E/(Tc^2)))))+2689)-
((32.508*log(10^(C+(D/Tc)+(E/(Tc^2)))))+2513.2))/100)*(T5-
Tc))+(32.508*log(10^(C+(D/Tc)+(E/(Tc^2)))))+2513.2
%Outlet temperature of hot water in generator
F=@(x) [((x(2)-f18*Cpw*(T18-x(1))));
  (x(2)-(UAg*((T18-x(3))-(x(1)-T5))/(log((T18-x(3))/(x(1)-T5)))));
(x(2)-(f6*(A6+((x(3)-273.2)*B6)+(C6*(x(3)-273.2)^2)))-(f1*h10)+(f5*h5))];
x0 = [352;296/2.89;65+273.2];          % Make a starting guess at the solution
Options = optimset('Display','iter');
E= fsolve(F,x0, Options)  % Call optimizer
T19=E(1,1);
Qg=E(2,1);
T6=E(3,1);
h6 =A6+((T6-273.2)*B6)+(C6*(T6-273.2)^2)
%Outputs
output(1)=T6;
output(2)=Qg;
output(3)=T19
  end
```

Appendix C

The MATLAB code for the latent heat storage :

```
clc
clear all
%%%PCM Storage
global L ro R N_z N_r N_t  rho_f mio_f Cp_f m_f k_f Np rho_pl rho_ps rho_pt Cp_ps Cp_pl delta_H T_m1
T_m2 k_ps k_pl k_pt dz dr dt h
%% Geometry parameters
L =  1.4                    %Length of Cylinder (m)
ro = 0.0055                 %Inside radius of the tube (m)
R =  0.045                  %Outside radius of the tube(m)
ratio = fix(L/(R-ro));
N_z = 320;                  %Number of points in x direction
N_r = fix(N_z/ratio)        %Number of points in r direction
time =11*3600
N_t =11*3600*0.03 ;     %time (second)
dt = time/(N_t-1);

%% Physical properties of HTF
rho_f =  985;                 %density (kg/m3)
mio_f = 4.92*10^-4;       %Dynamic viscosity of water (kg/m s)
Cp_f =  4178;               %Specific heat capacity (J/kg.K)
m_f = 0.201;                %Mass flow rate of HTF (kg/s)
k_f = 0.652;
Np=70;
 Re = 2*m_f/(pi*Np*ro*mio_f)     %Reynolds number
Pr = Cp_f*mio_f/k_f           %Prantel number
if Re<2200
   Nu = 3.66;
else
   if Re>5*10^6
      Nu = 0.023*Re^0.8*Pr^0.4;
   else
      if (Re >=2100)&& (Re<=5*10^6);
       f = ((0.79*log(Re))-1.64)^-2;
       Nu = ((f/8)*(Re-1000)*Pr)/(1+(12.7*((f/8)^0.5)*((Pr^(2/3))-1)));
      end
   end
end
h =Nu*k_f/(2*ro)          %Convective heat transfer coefficient (W/m2.k)

%%Physical properties of PCM (Erythritol)
rho_ps =  1480;             %density (kg/m3)
rho_pt =  1390;             %density (kg/m3)
rho_pl =  1300;             %density (kg/m3)
Cp_ps =  1.38*1000;       %Specific heat capacity (J/kg.K)
Cp_pl =  2.76*1000;       %Specific heat capacity (J/kg.K)
delta_H =  339.8*1000;    %Latent heat of fusion (J/kg)
T_m1 =  115.6+273.2;      %lower melting temperature (K)
T_m2 =  119.7+273.2;      %higher melting temperature (K)
k_ps =  0.733;              %solid Conductive heat transfer coefficient (W/mK)
k_pl =  0.326;              %liquid Conductive heat transfer coefficient (W/mK)
```

```
k_pt =  0.5295;                %transition phase Conductive heat transfer coefficient (W/mK)
%% Constants
j = 1:N_z;
k = 1:N_r;
dz = L/(N_z-1)
dr = (R-ro)/(N_r-1)
V = pi*(R^2-ro^2)*L;
%% Inlet temperature
T = ones((N_r*N_z)+N_z,N_t);
T (1:(N_r*N_z),1)=(20+273.2);
T ((N_r*N_z)+1:(N_r*N_z)+N_z,1)=(20+273.2);
Ti = 20+273.2;
T_inlet = 135+273.2*ones(1,N_t);
alfa = zeros((N_z*N_r),N_t);
alfa(:,1) = (rho_ps/k_ps)*Cp_ps;
K = zeros((N_z*N_r),N_t);
K(:,1) = k_ps;
Beta = zeros((N_z*N_r),1);
Beta(:,1) = 0;
i = zeros(((N_z-1)*(N_r-1)),N_t);
Tm = zeros(((N_z-1)*(N_r-1)),N_t);
e_l = zeros(((N_z-1)*(N_r-1)),N_t);
e_s = zeros(((N_z-1)*(N_r-1)),N_t);
Tmo = 20+273.2;
i(:,1) = Tmo*Cp_ps*10^-3;
e = zeros(((N_z-1)*(N_r-1)),N_t);

node_number = @(J0,K0) ((K0-1)*N_z)+J0;
cell_number = @(J0,K0) ((K0-1)*(N_z-1))+J0;
node_number_teta = @(J0,K0) (((K0-1)*N_z)+J0)+(N_r*N_z);
cell_number_teta = @(J0,K0) (((K0-1)*(N_z-1))+J0);
tic;


for k=1:N_r-1
   for j=1:N_z-1
      e(cell_number(j,k),1) = i(cell_number(j,k),1)*rho_ps*((((k*dr)+ro)^2)-((((k-1)*dr)+ro)^2))*pi*dz;
   end
end
for k=1:N_r-1
   for j=1:N_z-1
      v(cell_number(j,k),1) =((((k*dr)+ro)^2)-((((k-1)*dr)+ro)^2))*pi*dz;
   end
end
V = sum(v(:,1))*Np;
Vtot = pi*(R^2-ro^2)*L*Np;
E_pcm = zeros(1,N_t);
Eo = (sum(e(:,1)))*Np;
efficiency =zeros(1,N_t);
E_s = zeros(1,N_t);
E_l = zeros(1,N_t);
Q_f = zeros(1,N_t);
  for n=2:1:N_t
if rem(n,100)==0;display([num2str(n) 'th time step...']);
end
```

```
          [Tn,alfa_n,Beta_n,K_n] = PCM_Erythritol_ch(T(:,n-1),alfa(:,n-
1),Beta(:,n-1),T_inlet(n),n,K(:,n-1));

   T(:,n) = Tn;

   alfa(:,n) = alfa_n;
   Beta(:,n) = Beta_n;
   K(:,n) = K_n;
end

 for n=1:1:N_t
   for j=1:N_z-1
      for k=1:N_r-1
         Tm (cell_number(j,k),n)
=(T(node_number(j,k),n)+T(node_number(j+1,k),n)+T(node_number(j,k+1),n)+T(node_number(j+1,k+1),n))/4;
         if Tm (cell_number(j,k),n)<T_m1
            i(cell_number(j,k),n)= Cp_ps*10^-3* Tm (cell_number(j,k),n);
            e(cell_number(j,k),n)= i (cell_number(j,k),n)*rho_ps*((((k*dr)+ro)^2)-((((k-1)*dr)+ro)^2))*pi*dz;
            e_s(cell_number(j,k),n) = Cp_ps*10^-3* Tm (cell_number(j,k),n)*rho_ps*((((k*dr)+ro)^2)-((((k-
1)*dr)+ro)^2))*pi*dz;
            e_l (cell_number(j,k),n) = 0;
         else
            if (Tm (cell_number(j,k),n)>= T_m1) && (Tm (cell_number(j,k),n)<= T_m2)
               i(cell_number(j,k),n)= (Cp_pl* 10^-3*Tm (cell_number(j,k),n))+(delta_H*10^-3*(Tm
(cell_number(j,k),n)-T_m1)/(T_m2-T_m1));
               e(cell_number(j,k),n)= i (cell_number(j,k),n)*rho_pt*((((k*dr)+ro)^2)-((((k-1)*dr)+ro)^2))*pi*dz;
               e_s(cell_number(j,k),n) = Cp_pl*10^-3* Tm (cell_number(j,k),n)*rho_pt*((((k*dr)+ro)^2)-((((k-
1)*dr)+ro)^2))*pi*dz;
               e_l (cell_number(j,k),n) = (delta_H*10^-3*(Tm (cell_number(j,k),n)-T_m1)/(T_m2-
T_m1))*rho_pt*((((k*dr)+ro)^2)-((((k-1)*dr)+ro)^2))*pi*dz;
            else
               if Tm (cell_number(j,k),n)>T_m2
                  i(cell_number(j,k),n)= (Cp_pl*10^-3* Tm (cell_number(j,k),n))+(delta_H*10^-3);
                  e(cell_number(j,k),n)= i (cell_number(j,k),n)*rho_pl*((((k*dr)+ro)^2)-((((k-
1)*dr)+ro)^2))*pi*dz;
                  e_s(cell_number(j,k),n) = Cp_pl*10^-3* Tm (cell_number(j,k),n)*rho_pl*((((k*dr)+ro)^2)-((((k-
1)*dr)+ro)^2))*pi*dz;
                  e_l (cell_number(j,k),n) = (delta_H*10^-3)*rho_pl*((((k*dr)+ro)^2)-((((k-1)*dr)+ro)^2))*pi*dz;
               end
            end
         end
      end

  end

   E_pcm (1,n) =(sum(e(:,n)))*Np;
   efficiency (1,n)= (E_pcm(1,n)-Eo)/((V*10^-3*((rho_pl*Cp_pl*T_inlet(1,n))-
(rho_ps*Cp_ps*Ti)))+(V*rho_pl*delta_H*10^-3));
end
```

```
function [Tn,alfa_n,Beta_n,K_n]=PCM_Erythritol_ch(Tn_1,alfa,Beta,T_inlet,n,K)
%%PCM Storage
%% Geometry parameters
global L ro R N_z N_r N_t  rho_f mio_f Cp_f m_f k_f Np rho_pl rho_ps rho_pt Cp_ps Cp_pl delta_H T_m1
T_m2 k_ps k_pl k_pt dz dr dt h


a1 = 2*h/(rho_f*Cp_f*ro);
b1 = m_f/(Np*rho_f*pi*ro^2);
%solution
A = zeros(((N_z*N_r)+N_z),(N_r*N_z)+N_z);
j = 1:N_z;
k = 1:N_r;
r(k) = ((k-1)*dr)+ro;

%
node_number = @(J0,K0) ((K0-1)*N_z)+J0;
node_number_teta = @(J0,K0) (((K0-1)*N_z)+J0)+(N_r*N_z);
%%filling the Matrix for internal nodes

eq = 1;
for j = 2:N_z-1
   for k = 2:N_r-1
      N1 = node_number(j-1,k);
      N2 = node_number(j,k-1);
      N3 = node_number(j,k+1);
      N4 = node_number(j+1,k);
      N5 = node_number(j,k);
      %%
      A(eq,N1) = 1/(dz^2);
      A(eq,N2) = 2*(((k-2)*dr)+ro)/(((((k-1)*dr)+ro)^2-(((k-2)*dr)+ro)^2)*dr);
      A(eq,N3) = 2*(((k-1)*dr)+ro)/(((((k-1)*dr)+ro)^2-(((k-2)*dr)+ro)^2)*dr);
      A(eq,N4) = 1/(dz^2);
      A(eq,N5) = -2*((1/(((((k-1)*dr)+ro)-(((k-2)*dr)+ro))*dr))+(1/dz^2));
      eq = eq+1;
   end
end

%%Boundary conditions at the lower wall
eq_B_LW=eq;
for k = 2:N_r
   j = 1;
   N7 = node_number(j,k);
   A(eq_B_LW,N7) = 1;
   j = 2;
   N8 = node_number(j,k);
   A(eq_B_LW,N8) = -1;
   eq_B_LW = eq_B_LW+1;
end
eq_B_HW = eq_B_LW;
%%Boundary conditions at the higher wall
for k = 2:N_r
   j = N_z-1;
   N9 = node_number(j,k);
```

```
    A(eq_B_HW,N9) = -1;
    j = N_z;
    N10 = node_number(j,k);
    A(eq_B_HW,N10) = 1;
    eq_B_HW = eq_B_HW+1;
end
eq_B_OR = eq_B_HW;
%%Boundary condition at the outer radius-+

for j = 2:N_z-1;
    k = N_r-1;
    N11 = node_number(j,k);
    A(eq_B_OR,N11) = -1;
    k = N_r;
    N12 = node_number(j,k);
    A(eq_B_OR,N12) = 1;
    eq_B_OR = eq_B_OR+1;
end
eq_B_W=eq_B_OR;

%% Boundary condition of the wall
for j=1:N_z
    N13 = node_number(j,1);
    A(eq_B_W,N13) = -(h+(K (node_number(j,k))/dr));
    N14 = node_number(j,2);
    A(eq_B_W,N14) = (K (node_number(j,k))/dr);
    N15 = node_number_teta(j,1);
    A(eq_B_W,N15)=h;
    eq_B_W = eq_B_W+1;
end
eq_B_HTF = eq_B_W;

%% Pipe (HTF)

for j = 2:N_z
    N16 = node_number_teta(j-1,1);
    A(eq_B_HTF,N16) = b1/dz;
    N17 = node_number_teta(j,1);
    A(eq_B_HTF,N17) = -(a1+(b1/dz));
    N18 = node_number(j,1);
    A(eq_B_HTF,N18) = a1 ;
    eq_B_HTF = eq_B_HTF+1;
end
%% inlet of the pipe j=1
N19 = node_number_teta(1,1);
A(eq_B_HTF,N19) = 1;



%% Forming Matrix B(Matrix coefficient for n)
tic;
B = zeros(((N_z*N_r)+N_z),(N_r*N_z)+N_z);
eq_B=1;
for j=2:N_z-1
    for k=2:N_r-1
```

```
        B(eq_B,node_number(j,k)) = (-1/dt)*alfa(node_number(j,k));
        eq_B=eq_B+1;
    end
end


%%HTF
eq_B_WB = eq_B_W;
for j=2:N_z
    B(eq_B_WB,node_number_teta(j,1)) = (-1/dt)*1;
    eq_B_WB=eq_B_WB+1;
end

%%Forming Matrix Beta at time n

D = zeros(((N_z*N_r)+N_z),1);
for j=2:N_z-1
    for k=2:N_r-1
        D(node_number(j,k)) = (-1/dt)*Beta(node_number(j,k));
    end
end

%% Forming Matrix E(Matrix coefficient for n-1)

E = zeros(((N_z*N_r)+N_z),(N_r*N_z)+N_z);
eq_E=1;
for j=2:N_z-1
    for k=2:N_r-1
        E(eq_E,node_number(j,k)) = (1/dt)*alfa(node_number(j,k));
        eq_E=eq_E+1;
    end
end

%%Pipe
eq_B_WE=eq_B_W;
for j=2:N_z
    E(eq_B_WE,node_number_teta(j,1)) = (1/dt)*1;
    eq_B_WE=eq_B_WE+1;
end

%%Forming Matrix Beta at time n-1

G= zeros(((N_z*N_r)+N_z),1);
for j=2:N_z-1
    for k=2:N_r-1
        G(node_number(j,k)) = (1/dt)*Beta(node_number(j,k));
    end
end

%%

F=zeros((N_r*N_z)+N_z,1);
F((N_r*N_z)+N_z,1)=T_inlet;

%%
```

```
Tn=(A+B)\((-E*Tn_1)+F-G-D);

%%
for j=1:N_z
   for k=1:N_r
      if Tn(node_number(j,k),1)<T_m1
         alfa_n(node_number(j,k),1) = (rho_ps/k_ps)*Cp_ps;
         Beta_n(node_number(j,k),1) = 0;
         K_n(node_number(j,k),1)=k_ps;

      else
         if (Tn(node_number(j,k),1)>= T_m1) && (Tn(node_number(j,k),1)<= T_m2)
            alfa_n(node_number(j,k),1) =(rho_pt/k_pt)*(Cp_pl+(delta_H/(T_m2-T_m1)));
            Beta_n(node_number(j,k),1) = (rho_pt/k_pt)*(-delta_H*T_m1/(T_m2-T_m1));
            K_n(node_number(j,k),1)=k_pt;

         else
            if Tn(node_number(j,k),1)>T_m2
               alfa_n(node_number(j,k),1) = (rho_pl/k_pl)*Cp_pl;
               Beta_n(node_number(j,k),1) = (rho_pl/k_pl)*delta_H;
               K_n(node_number(j,k),1)=k_pl;

            end
         end
      end
   end
end

end
```